
Adaptive Rank, Reduced Forgetting: Continual Learning with Dynamic Rank-Selective LoRA

Haodong Lu^{1,2} Chongyang Zhao¹ Jason Xue²

Lina Yao¹ Kristen Moore² Dong Gong^{1*}

¹University of New South Wales, ²CSIRO’s Data61

{haodong.lu, chongyang.zhao, lina.yao, dong.gong}@unsw.edu.au,
{jason.xue, kristen.moore}@data61.csiro.au

Abstract

Continual learning (CL) aims to accumulate knowledge from sequential tasks without catastrophic forgetting. Many CL methods for pre-trained models (PTMs) achieve strong performance but rely on sophisticated architectures or additional assumptions. They adapt isolated modules—adding inference complexity and limiting PTM improvement—or depend on replay, stored data, or assumptions, incurring extra cost and reduced applicability. To advance usage, we explore natural, efficient PTM CL instead of complex task-specific additions. We study continual low-rank learning and systematically analyze how LoRA ranks and placements affect learning and forgetting. We find that a relatively higher-rank LoRA improves task learning (*i.e.*, *plasticity*) but increases forgetting, while lower-rank LoRA reduces forgetting (*i.e.*, *stability*) but limits adaptation. Crucially, we observe a *plasticity–stability balance* tied to ranks across parameters and tasks, with *moderately small ranks* maximizing CL benefits. Motivated by this, we propose **Continual Dynamic Rank-Selective LoRA (CoDyRA)**, continually updating PTMs with LoRA of adaptively optimized ranks. While the new-task objective drives learning, CoDyRA adaptively minimizes ranks with *sparsity-promoting regularization* to reduce interference and forgetting, achieving plasticity–stability balance adaptively for different parameters and tasks. It preserves the original model architecture and serving pipeline, adding no inference overhead. Extensive experiments on both CLIP and LLMs show CoDyRA improves new-task learning with strong knowledge retention, delivering state-of-the-art results. [Code](#) is available.

1 Introduction

Continual learning (CL) [11, 23, 77] focuses on incrementally learning from new data streams without catastrophic forgetting [51, 56] or the need to retrain on all previously seen data. With the rise of pre-trained models (PTMs), recent studies increasingly perform CL in this context [32, 52, 75, 103]. Following the context of class-incremental learning (CIL) tasks [68, 85], many PTM-based CL approaches primarily focus on or are evaluated through continual adaptation to downstream tasks. While task-specific and downstream-oriented designs [52, 90, 93, 103] show promising results on particular CL tasks, PTMs remain largely isolated from the CL process, mitigating forgetting but undermining interaction with new tasks and thus the potential for continual improvement. To advance toward models that function as continual learners, we consider CL with PTMs that enable flexible and efficient updates, preserving or even enhancing generalizable representations while acquiring new knowledge.

*D. Gong is the corresponding author. H. Lu is supported by a CSIRO’s scholarship.

Leveraging the strong generalization and flexibility of jointly learned vision–text embeddings, CLIP as a vision–language model has been widely adopted in CL [32, 79, 99, 102], including continual updating [21] and multi-domain CL [99]. Beyond downstream performance, the retention of knowledge in PTMs is also evaluated. Some approaches, such as ZSCL [99], aim to continually update the pretrained CLIP through full fine-tuning while mitigating forgetting via memory replay [38, 64, 85] using additional reference data. However, this leads to high training costs and still struggles with catastrophic forgetting (Fig. 1(a)). To directly control the forgetting, some methods [90, 93] introduce task-specific components isolated from the frozen PTMs, requiring task/domain prediction or gating for routing the specific components at inference. These methods can deliver strong results with task-specific gating and branching; however, by isolating tasks and relying heavily on per-task modules and accurate task prediction, they become restricted to certain domains and limited in both general CL applicability and inference efficiency. Moreover, the restricted interaction between PTMs and CL process (e.g., isolation) limits PTMs’ generalization improvement potential (Fig. 1(b)).

General-purpose PTM updating can be achieved through direct model updating via straightforward full fine-tuning (FT) or parameter-efficient fine-tuning (PEFT) methods [104, 105], such as Low-Rank Adaptation (LoRA) [27]. This raises a fundamental question: instead of relying on complex additions or task-specific components, *can CL be performed by leveraging these natural PTM update mechanisms?* Our work investigates how to mitigate catastrophic forgetting within these standard frameworks without imposing additional assumptions. We propose an efficient CL approach for CLIP that enables the model to be updated naturally across a stream of tasks, while retaining foundational pretrained knowledge. We build upon LoRA for efficiency. There have been some LoRA-based CL methods [40, 87, 106], which rely on specific regularization (e.g., orthogonal property) for specific settings.

We first systematically analyze and ablate how LoRA adapters at different locations in the network with different ranks influence learning and forgetting (Sec. 3.2). Our analyses reveal that *not all* LoRA ranks and placements contribute *equally* to downstream learning and forgetting. Our analyses empirically demonstrate that, for arbitrary weights, *relatively higher-rank* LoRA facilitates learning new tasks (*i.e.*, *plasticity*) but tends to increase forgetting, while *lower-rank* LoRA mitigates forgetting (*i.e.*, *stability*) but limits adaptation. Importantly, we identify that there exists a **balance between *plasticity* (learning new knowledge) and *stability* (regularizing forgetting)** at a moderately small (but not too small) rank, potentially maximizing CL benefits. Moreover, we observe that this balance *varies* significantly across different parameter placements.

The analysis results motivate us to propose **Continual Dynamic Rank-Selective LoRA (CoDyRA)**, which continually updates the PTM using LoRA adapters with dynamically and adaptively optimized ranks. CoDyRA performs *new task learning* while jointly *minimizing the rank* of each LoRA adaptively. Rank selection is guided by *sparsity-promoting regularization* and learnable importance weights, which dynamically adjust the contribution of each rank and decide a balanced capacity in training. By updating with LoRA adapters of minimized ranks, CoDyRA inherently regularizes models toward remaining closer to their previous state, thereby alleviating forgetting in principle without task-specific assumptions.

Our contributions are fourfold: (1) We study PTM-based CL with natural and efficient continual update of the model, not relying on complex task-specific additions, without storing past data, task information, or relying on assumptions. (2) We comprehensively analyze learning–forgetting trade-

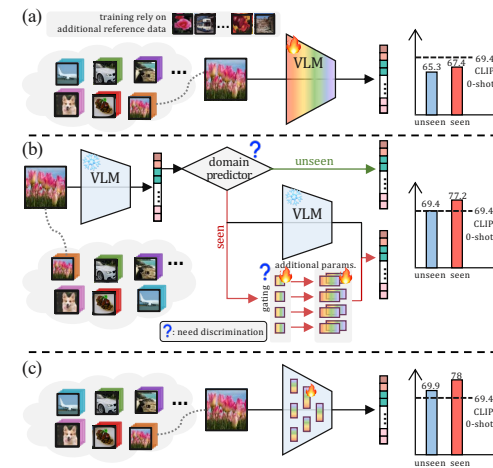


Figure 1: (a) Continual full fine-tuning leverages reference data to reduce forgetting of pre-trained knowledge (e.g., zero-shot performance [99]) but remains costly and prone to forgetting. (b) Task-specific modular methods (e.g., [90, 93]) add isolated components requiring domain prediction or gating, increasing complexity and limiting adaptability and generalization. (c) Our approach enables efficient, universal continual PTM updating without reference data or task-specific designs, retaining PTM knowledge and improving performance on unseen data.

offs across LoRA ranks and placements, identifying a plasticity–stability balance at moderately small ranks and deriving design strategies. This study guides our CL approach with regularized forgetting and provides evidence for future research. (3) We propose CoDyRA, which adaptively minimizes LoRA ranks via sparsity-promoting regularization. It handles different parameters and tasks, yielding regularized updates that reduce interference and keep the model closer to its previous state with less forgetting. (4) Extensive experiments across multiple CL benchmarks demonstrate superior downstream performance and reduced forgetting, achieving a strong plasticity–stability balance. We further extend CoDyRA to LLMs beyond CLIP, validating its effectiveness on broader applications and pre-trained models.

2 Related Work

Continual Learning. Continual learning enables models to sequentially learn new tasks while retaining previously acquired knowledge. Experience replay (ER) methods [3, 8, 9, 42, 48, 91, 92] store subsets of past data to refresh the model on prior tasks during new training. Parameter regularization approaches [1, 2, 31, 33, 39, 94] constrain updates to important weights to preserve past knowledge. Dynamic networks [40, 52, 65, 68, 73–75, 82–84, 101] adjust their architecture on the fly, balancing the acquisition of new information with the retention of old knowledge.

Continual Learning of CLIP. CL of CLIP [32, 97] aims to enable PTMs to sequentially learn across diverse domains while retaining their pre-trained generalization capabilities for previously seen tasks. [21] continually adapt CLIP to temporal distribution shifts via timestamped data updates. ZSCL [99] was proposed to address catastrophic forgetting while preserving zero-shot capabilities during task adaptation. Subsequent works [29, 41, 69, 90, 93] have focused primarily on continual adaptation to downstream tasks while leveraging pre-trained predictions for unseen data. Recently, a more challenging setting was proposed, where the labels from different domains are mixed during testing [90].

Low-Rank Adaptation. Low-Rank Adaptation (LoRA) [27] has gained popularity as a parameter-efficient method for fine-tuning large pre-trained models. Similar to LoRA, [88] learns a small set of task-specific representation vectors at each layer. Building on LoRA’s framework, recent works enhance LoRA by reformulating parameter updates, focusing on initialization based on the pre-trained weights [53, 95], treating each rank independently [14, 43, 96], or employing a mixture of subspaces [86]. LoRA has been shown to be effective even with small ranks [5, 66], while our work investigates how to perform low-rank learning in CL and how to dynamically and adaptively decide capacity. Owing to their effectiveness and efficiency, LoRA-based methods have been extended to CL of LLMs, often relying on specialized regularization or architectural designs [60, 61, 80]. For instance, O-LoRA [80] mitigates interference via orthogonal regularization; TreeLoRA [60] routes inputs to task-specific adapters using a gradient-similarity tree with bandit search.

3 Methodology

3.1 Preliminaries

Transformers. A typical transformer model is composed of stacked blocks, each containing two main submodules: an multi-head attention (MHA) module (Attn) and a multilayer perceptron (MLP). The attention module at the l -th layer is defined as: $\text{Attn}(x) = \text{MHA}(x\mathbf{W}_l^Q, x\mathbf{W}_l^K, x\mathbf{W}_l^V)\mathbf{W}_l^O$. The input sequence is denoted as $x \in \mathbb{R}^{n \times d}$, where n is the sequence length and d is the hidden dimension. The matrices $\mathbf{W}_l^Q, \mathbf{W}_l^K, \mathbf{W}_l^V, \mathbf{W}_l^O \in \mathbb{R}^{d \times d}$ correspond to the Query, Key, Value, and Output projection matrices, respectively. The MLP in each transformer block consists of two linear layers separated by an activation function $\text{Act}(\cdot)$, such as ReLU or GELU [26]. The MLP module at the l -th transformer layer is defined as: $\text{MLP}(x) = \text{Act}(x\mathbf{W}_l^{\text{FC}} + b_l^{\text{FC}})\mathbf{W}_l^{\text{Proj}} + b_l^{\text{Proj}}$, where $\mathbf{W}_l^{\text{FC}} \in \mathbb{R}^{d \times d_m}$ and $\mathbf{W}_l^{\text{Proj}} \in \mathbb{R}^{d_m \times d}$ are the weight matrices, with d_m being the hidden dimension.

CLIP model. In CLIP [17, 30, 62], both the image encoder f_θ and text encoder g_ψ are transformers that learn a joint vision–language embedding. Given an image $\mathbf{x} \in \mathbb{R}^{H \times W \times C}$, the vision encoder produces features $\mathbf{z}_V = f_\theta(\mathbf{x}) \in \mathbb{R}^D$. A class label y is embedded into a prompt such as “a photo of a [CLS]” to form text input \mathbf{t} , which the text encoder maps to $\mathbf{z}_T = g_\psi(\mathbf{t}) \in \mathbb{R}^D$. At inference, the

probability of classifying \mathbf{x} into class $y_i \in \{1, \dots, C\}$ is: $p(y_i|\mathbf{x}) = \frac{\exp(\text{sim}(\mathbf{z}_V, \mathbf{z}_T^{y_i})/\tau)}{\sum_{c=1}^C \exp(\text{sim}(\mathbf{z}_V, \mathbf{z}_T^{y_c})/\tau)}$, where $\text{sim}(\cdot)$ is cosine similarity and τ is a temperature parameter.

CL with CLIP. We study continual learning of CLIP with multi-domain data, *e.g.*, multi-domain task-incremental learning (MTIL) [93, 99] and cross-domain task-agnostic incremental learning (X-TAIL) [90]. In MTIL, the model sequentially learns from T tasks, where each task t has dataset $\mathcal{D}^t = \{(\mathbf{x}_i^t, y_i^t)\}_{i=1}^{N^t}$, with input image $\mathbf{x}_i^t \in \mathbb{R}^{H \times W \times C}$, label $y_i^t \in \mathcal{C}^t$, and M^t classes in $\mathcal{C}^t = \{y_j^t\}_{j=1}^{M^t}$. In X-TAIL, the test-time category set includes both seen and unseen domains, $\mathcal{C} = \mathcal{C}_{\text{seen}} \cup \mathcal{C}_{\text{unseen}}$, where $\mathcal{C}_{\text{seen}} = \bigcup_{i=1}^n \mathcal{C}_i$ contains all classes from prior tasks and $\mathcal{C}_{\text{unseen}}$ denotes novel classes never encountered.

3.2 Analyses on LoRA Location and Rank

To enable efficient and natural continual updating of PTMs, we employ LoRA and analyze its learning and forgetting capability for optimizing its usage. We examine how LoRA’s rank and placement affect downstream learning and forgetting through two types of analyses [54, 59], providing a comprehensive view of their overall impact. (1) We first apply LoRA components with varying ranks at different locations in the pre-trained CLIP, for measurement of importance or contribution (Fig. 2); (2) We apply LoRA across all PTM weights and systematically prune them for evaluation, for testing the standalone capability (Fig. 3). We train the model on downstream datasets and assess its performance on both (1) the new task, *i.e.*, learning new knowledge, and (2) an additional reference dataset to evaluate the retention and forgetting of existing capabilities. Without loss of generality, the learning-forgetting analyses can be extended to each learning step in straightforward, assumption-free CL.

Applying LoRA on all weights. Unlike prior works [27, 53, 95] that only apply LoRA to limited components by default, we first examine the impact of different LoRA placements. As shown in Fig. 2 and Fig. 3, applying LoRA to only specific modules alone may limit learning capacity in different ways: (1) LoRA placement strongly impacts downstream performance and retention of pre-trained capabilities; (2) Updating only the vision encoder causes more forgetting; (3) Updating only attention modules mitigates forgetting but limits learning on new tasks. These observations reflect the distinct roles of PTM components. **Take-away 1:** Instead of manual or fixed LoRA placement [27, 53, 95], we apply LoRA to all weights and optimize for an *adaptive* configuration.

The effects of LoRA ranks on balancing learning and forgetting. We identified the rank number of LoRA plays a critical role for balancing learning and forgetting. As shown in Fig. 2, we can observe that a relatively higher-rank LoRA facilitates learning new tasks but tends to increase forgetting, while a lower-rank LoRA mitigates forgetting but limits adaptation. This suggests that lower-rank LoRA interferes less with existing knowledge (*i.e.*, reduces forgetting) while learning less new knowledge. Fortunately, we identify a *balance* (top-right in Fig. 2), where a moderately small rank reduces forgetting while enabling enough adaptability.

During training, low-rank updates tend to enable the updated model to be closer to the original model, with less interference and forgetting. In the extreme case, a rank-zero LoRA learns nothing and introduces no forgetting. Thus, minimizing LoRA rank for each new task in CL can reduce forgetting without extra assumptions. On the other hand, the task-learning objective emphasizes new knowledge

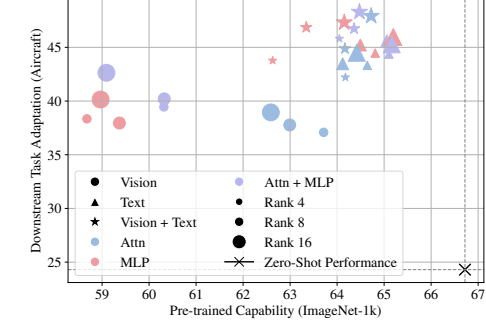


Figure 2: Task adaptation and zero-shot capability retention after training CLIP with different LoRA insertion points and ranks. Shapes indicate encoders, colors denote transformer modules, and sizes reflect rank values.

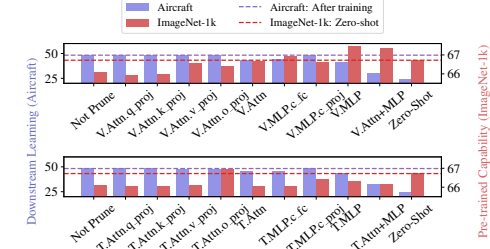


Figure 3: Impact of removing trained LoRA modules on downstream task adaptation (Aircraft, left y-axis) and retention of existing capabilities (ImageNet-1k, right y-axis). “T” and “V” indicate text-encoder and vision-encoder modules, respectively.

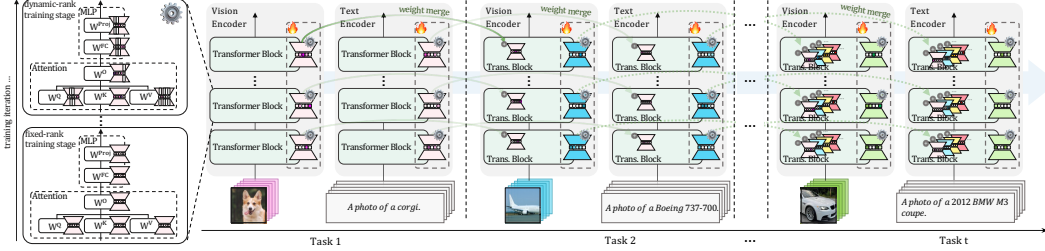


Figure 4: Overview of CoDyRA: we propose dynamic rank-selection LoRA, enabling each pre-trained weight matrix to adaptively add necessary ranks for downstream adaptation while retaining pre-trained capabilities. After each task, dynamic rank updates are merged into the pre-trained weights with no inference overhead.

acquisition, enabling a balance. **Takeaway 2:** A **plasticity–stability balance** exists and associates with LoRA rank (high vs. low), which can be adaptively achieved by jointly **optimizing the task objective** and **minimizing LoRA ranks**.

The balance varies by location and task. Fig. 2 shows that the optimal rank for balance depends on both parameter placement and the learning task, consistent with the pruning-based sufficiency analysis in Fig. 3. For example, removing updates to the Value projection in the Attention module of the vision encoder had little impact on adaptation but substantially restored pre-trained performance. Interestingly, pruning the MLP layer slightly reduced task performance while enhancing pre-trained capabilities. **Takeaway 3:** The **learning–forgetting** balance point tied to rank varies across modules and tasks, necessitating adaptive optimization.

3.3 Proposed CoDyRA with Sparsity-Induced Rank Selection and Minimization

Overview. Our analyses in Sec. 3.2 suggest applying LoRA across all CLIP modules while adaptively optimizing for an appropriate rank for each specific task and location to balance learning and forgetting. Together with the task learning objective, minimizing active LoRA ranks acts as a regularizer, keeping the updated model closer to its previous state and alleviating forgetting. However, the balanced rank between learning and forgetting is not consistent across parameters or tasks (**Takeaway 3**). We address this with a sparsity-promoting regularization for the LoRA adapters.

We introduce adaptive rank-selective updates for all pre-trained weight matrices in the Attention and MLP modules of both vision and text encoders (Fig. 4). The sparsity-promoting regularization enables adaptive rank selection and minimization for each LoRA adapter on each task. For each task in CL, beyond adaptive rank minimization, CoDyRA requires no additional priors or assumptions and does not store or maintain information (e.g., data, parameters, or statistics) from previous steps, unlike prior methods [90, 93, 99].

During training on task t , we denote the pre-trained weights, or those updated from previous tasks, as $\{\mathbf{W}_0^{t,m}\}_{m=1}^M$, where M is the total number of weight matrices updated by LoRA. After each task, the dynamic rank updates are merged back into the original weights.

Regularized low-rank updates with rank importance. To update weight matrix $\mathbf{W}_0^{t,m} \in \mathbb{R}^{d \times k}$, LoRA [27] introduces two low-rank matrices, $\mathbf{B}^{t,m} \in \mathbb{R}^{d \times r}$ and $\mathbf{A}^{t,m} \in \mathbb{R}^{r \times k}$, such that $\Delta \mathbf{W}^{t,m} = \mathbf{B}^{t,m} \mathbf{A}^{t,m}$, where $r \ll \min(d, k)$. The updated weight matrix is defined as:

$$\mathbf{W}^{t,m} = \mathbf{W}_0^{t,m} + \Delta \mathbf{W}^{t,m} = \mathbf{W}_0^{t,m} + \mathbf{B}^{t,m} \mathbf{A}^{t,m}. \quad (1)$$

Only $\mathbf{B}^{t,m}$ and $\mathbf{A}^{t,m}$ are trained for each task and then merged into the weights. LoRA incurs no additional computational overhead during inference.

As shown in Sec. 3.2, minimizing the active rank for each LoRA adapter alleviates forgetting, which can be formulated as minimizing a regularizer $R(\Delta \mathbf{W}^{t,m}) \doteq R(\mathbf{B}^{t,m} \mathbf{A}^{t,m})$. The minimum of $R(\Delta \mathbf{W}^{t,m})$ is zero, i.e., $\min R(\Delta \mathbf{W}^{t,m}) = 0$, corresponding to a rank-zero matrix—no update to $\mathbf{W}^{t,m}$ and hence no forgetting. By jointly optimizing the **new-task learning** objective and the **minimized $R(\Delta \mathbf{W}^{t,m})$** , we achieve a balance between **learning** and **forgetting**.

To automatically and adaptively minimize the active ranks in LoRA, we formulate $R(\Delta \mathbf{W}^{t,m})$ through a rank-selection LoRA. We introduce a learnable importance weight vector $\mathbf{w}^{t,m} \in \mathbb{R}^r$ to indicate the active ranks for a LoRA adapter:

$$\Delta \mathbf{W}^{t,m} = \sum_{i=1}^r \mathbf{w}_i^{t,m} \mathbf{B}_{:,i}^{t,m} \mathbf{A}_{i,:}^{t,m} \quad (2)$$

where $\mathbf{w}_i^{t,m}$ is the learnable importance weight associated with rank i , $\mathbf{B}_{:,i}^{t,m}$ denotes the i -th column of $\mathbf{B}^{t,m}$, and $\mathbf{A}_{i,:}^{t,m}$ denotes the i -th row of $\mathbf{A}^{t,m}$. Minimizing $R(\Delta \mathbf{W}^{t,m})$ can be achieved through optimizing $\mathbf{w}^{t,m}$.

Adaptive rank-selective updates with sparse-promoting regularization. The formulation in Eq. (2) enables the model to dynamically optimize the importance of each rank and minimize active ranks through gradient descent. To only retain the essential ranks for learning new tasks (thus reducing forgetting), we can achieve optimizing $R(\Delta \mathbf{W}^{t,m})$ through an ℓ_1 norm-based sparsity-promoting regularization [14, 71] on $\mathbf{w}^{t,m}$, *i.e.*, $\|\mathbf{w}^{t,m}\|_1$. The optimization objective for parameters $\{\mathbf{w}^{t,m}, \mathbf{B}^{t,m}, \mathbf{A}^{t,m}\}_{m=1}^M$ learned on task t is:

$$\mathcal{L}_{\text{train}}^t := \mathcal{L}_{\text{sup}}^t + \lambda \sum_{m=1}^M \|\mathbf{w}^{t,m}\|_1, \quad (3)$$

where $\mathcal{L}_{\text{sup}}^t$ is the supervised training loss for current task, M is the number of weight matrices inserted r -rank update, and $\mathbf{w}^{t,m}$ represents the importance weights of each rank added to the weight matrix $\mathbf{W}_0^{t,m}$. The ℓ_1 regularization strength is controlled by λ . Minimizing $\|\mathbf{w}^{t,m}\|_1$ encourages minimizing of $\|\Delta \mathbf{W}^{t,m}\|_F$ if given $\mathbf{A}^{t,m}$ and $\mathbf{B}^{t,m}$ (according to Eq. (2)). It softly reduces capacity in updates conflicting with critical information encoded in the learned parameters, without introducing additional assumptions. More discussions are in Appendix A.3.

To handle the non-differentiable ℓ_1 regularization applied to the importance weights, we adopt the proximal gradient method [4]. The i -th element of $\hat{\mathbf{w}}^{t,m}$ for rank i is updated via soft-thresholding:

$$\mathbf{w}_i^{t,m} := \mathbb{1}(|\hat{\mathbf{w}}_i^{t,m}| > \kappa) \cdot (\hat{\mathbf{w}}_i^{t,m} - \text{sign}(\hat{\mathbf{w}}_i^{t,m}) \cdot \kappa), \quad (4)$$

where $\hat{\mathbf{w}}_i^{t,m}$ denotes the value of $\mathbf{w}_i^{t,m}$ after applying the gradient update from the supervised loss $\mathcal{L}_{\text{sup}}^t$. The threshold κ increases from zero to κ_{\max} , analogous to linearly scheduling λ , and adaptively induces sparsity in \mathbf{w} based on the task learning objective. The indicator $\mathbb{1}(\cdot)$ returns 1 if the condition holds and 0 otherwise, while $\text{sign}(\cdot)$ gives the input's sign (\pm). More details are left in Appendix A.

This approach preserves only the ranks with significant importance for learning current task and prunes those with low relevance, adapting across weights and tasks. The importance weights on preserved ranks softly highlight their relative significance. Early in training, dense updates are applied without Eq. (4), allowing all ranks to capture task-relevant information before sparsity is enforced.

Continual learning framework. For each task, we initialize and optimize CoDyRA modules, low-importance ranks are pruned via sparsity-promoting regularization, and remaining active ranks are merged into the backbone weights after training. This regularization naturally constrains update capacity, preserving prior knowledge while enabling efficient adaptation. Following standard conventions, we initialize LoRA matrix $\mathbf{A}^{t,m}$ randomly and $\mathbf{B}^{t,m}$ to zero, and our proposed importance $\mathbf{w}^{t,m}$ is randomly initialized.

4 Experiments

We evaluate our approach on continual learning tasks for both vision-language models and LLMs. For vision-language CLIP [30, 62] model, we utilize the MTIL [99] and X-TAIL [90] benchmarks. For LLMs, we assess performance on the TRACE benchmark [81] using LLaMA [16, 72] and Gemma [70]. Detailed experiment settings and additional results are provided in Appendix B.

4.1 Experimental Results

Experiments on CLIP continual learning. We evaluate performance on the MTIL benchmark in Table 1, reporting *Transfer* (retention on unseen tasks), *Last* (final task performance), and *Average* accuracy. Unlike prior methods [90, 93] that rely on frozen zero-shot predictions, effectively capping performance at the pre-trained level, CoDyRA continually updates the model, surpassing the zero-shot

Table 1: Comparisons on 5-shot MTIL setting. The **best** and the **second best** results are highlighted in **red** and **blue**, respectively. Methods marked with \dagger indicate the use of domain prediction or distribution detection [90, 93].

Method	Aircraft	Caltech101	CIFAR100	DTD	EuroSAT	Flowers	Food	MNIST	OxfordPet	Cars	SUN397	Average
CLIP												
Zero-shot [62]	24.3	88.4	68.2	44.6	54.9	71.0	88.5	59.4	89.0	64.7	65.2	65.3
<i>Transfer</i>												
Zero-shot [62]	—	88.4	68.2	44.6	54.9	71.0	88.5	59.6	89.0	64.7	65.2	69.4
LwF [38]	—	72.1	49.2	35.9	44.5	41.1	66.6	50.5	69.0	19.0	51.7	50.0
LwF-VR [15]	—	82.2	62.5	40.1	40.1	56.3	80.0	60.9	77.6	40.5	60.8	60.1
WISE-FT [85]	—	77.6	60.0	41.3	39.4	53.0	76.6	58.1	75.5	37.3	58.2	57.7
ZSCL [99]	—	84.0	68.1	44.8	46.8	63.6	84.9	61.4	81.4	55.5	62.2	65.3
MoE-Adapter \dagger [93]	—	87.9	68.2	44.1	48.1	64.7	88.8	69.0	89.1	64.5	65.1	68.9
RAIL-Primal \dagger [90]	—	88.4	68.2	44.6	54.9	71.0	88.5	59.6	89.0	64.7	65.2	69.4
CoDyRA	—	92.4	68.4	45.8	54.5	69.6	87.4	65.2	88.5	64.2	64.5	69.9
CoDyRA \dagger	—	92.4	68.4	45.8	54.5	69.6	87.4	65.2	88.5	64.2	64.5	69.9
<i>Average</i>												
LwF [38]	23.5	77.4	43.5	41.7	43.5	52.2	54.6	63.4	68.0	21.3	52.6	49.2
LwF-VR [15]	24.9	89.1	64.2	53.4	54.3	70.8	79.2	66.5	79.2	44.1	61.6	62.5
WISE-FT [85]	32.0	87.7	61.0	55.8	68.1	69.3	76.8	71.5	77.6	42.0	59.3	63.7
ZSCL [99]	28.2	88.6	66.5	53.5	56.3	73.4	83.1	56.4	82.4	57.5	62.9	64.4
MoE-Adapter \dagger [93]	30.0	89.6	73.9	58.7	69.3	79.3	88.1	76.5	89.1	65.3	65.8	71.4
RAIL-Primal \dagger [90]	32.9	94.5	69.9	58.1	71.8	84.4	88.5	70.4	89.0	66.1	65.7	71.9
CoDyRA	34.6	95.8	73.9	60.0	77.1	81.3	86.6	75.9	89.9	66.1	65.3	73.3
CoDyRA \dagger	37.6	96.0	76.6	62.1	78.7	82.0	86.8	76.0	90.0	66.2	65.3	74.3
<i>Last</i>												
LwF [38]	22.1	58.2	17.9	32.1	28.1	66.7	46.0	84.3	64.1	31.5	60.1	46.5
LwF-VR [15]	22.9	89.8	59.3	57.1	57.6	79.2	78.3	77.7	83.6	60.1	69.8	66.9
WISE-FT [85]	30.8	88.9	59.6	60.3	80.9	81.7	77.1	94.9	83.2	62.8	70.0	71.9
ZSCL [99]	26.8	88.5	63.7	55.7	60.2	82.1	82.6	58.6	85.9	66.7	70.4	67.4
MoE-Adapter \dagger [93]	30.1	89.3	74.9	64.0	82.3	89.4	87.1	89.0	89.1	69.5	72.5	76.1
RAIL-Primal \dagger [90]	32.9	95.1	70.3	63.2	81.5	95.6	88.5	89.7	89.0	72.5	71.0	77.2
CoDyRA	31.6	95.5	72.8	63.5	85.0	89.7	85.0	94.7	93.2	73.6	73.0	78.0
CoDyRA \dagger	37.6	96.4	78.4	68.2	92.6	92.3	86.2	94.9	93.8	75.2	73.0	80.8

upper bound in *Transfer* accuracy. While updates introduce minor perturbations, they ultimately enhance generalization. Regarding *Last* accuracy, we match or exceed baselines without relying on domain ID prediction [93] or memory banks [90]. As these architectural additions are orthogonal to our parameter-efficient approach, they can be integrated to further boost performance (e.g., CoDyRA \dagger employs domain-wise autoencoders). Extended results on X-TAIL (Table 5) and full-shot MTIL (Table 7) are detailed in Appendix B.4.

Experiments on language model continual learning. Table 2 evaluates CoDyRA on the TRACE benchmark [81] using LLaMA [16, 72] and Gemma [70]. Traditional regularization (EWC [33], OGD [18]), rehearsal (GEM [44]), and prompt-based methods (L2P [84], Dual-Prompt [83]) often underperform simple In-Context Learning (ICL [7]). Among parameter-efficient approaches, naive SeqLoRA suffers from significant forgetting. While O-LoRA [80], HiDeLoRA [76, 78], and TreeLoRA [60] improve stability, they impose rigid orthogonality, complex decomposition, or structural expansion. In contrast, CoDyRA achieves state-of-the-art performance without such constraints. By leveraging adaptive rank selection via sparsity-promoting regularization, it dynamically allocates capacity (minimizing ranks for stability while expanding for plasticity) to optimize the trade-off between learning and forgetting.

4.2 Discussions

Pre-trained knowledge retention and potential improvement. We assess transfer capability on unseen datasets: CIFAR100 [35], Places365 [100], and ImageNet-1k [12] (Table 3). Unlike prior methods [90, 93] that freeze the backbone and remain bounded by CLIP’s initial zero-shot

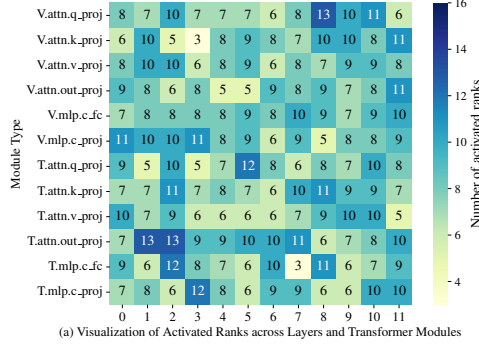
Table 3: Pre-trained retention on unseen datasets.

Method	Zero-shot Retention on Unseen Data			
	CIFAR100	Places365	ImageNet-1k	Average
Zero-Shot [62]	68.24	33.77	66.72	56.24
MoE-Adapter [93]	68.24	33.77	66.72	56.24
RAIL [90]	68.24	33.77	66.72	56.24
CoDyRA	68.95	36.52	68.52	58.00

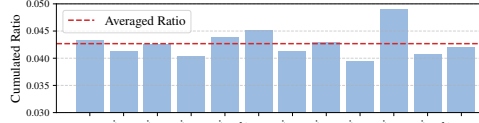
performance, CoDyRA continually integrates new knowledge into the parameter space. This allows our model to surpass the original zero-shot baseline, demonstrating that CoDyRA effectively expands general knowledge and potentially improves overall representations.

Table 2: Comparison with a broad range of CL methods on the TRACE benchmark. We report Overall Performance (OP (%) \uparrow) and Backward Transfer (BWT (%) \downarrow). Results are averaged over three runs with standard deviations. The best results are highlighted in bold.

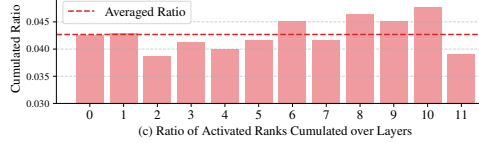
	FIX(ICL)	SeqLoRA	OGD	GEM	EWC	L2P	DualPrompt	HiDeLoRA	O-LoRA	TreeLoRA	CoDyRA
meta-llama / LLaMA-2-7B-Chat											
OP	38.94 \pm 0.3	34.3 \pm 1.2	42.09 \pm 1.6	40.08 \pm 1.6	42.36 \pm 1.2	36.23 \pm 0.8	37.69 \pm 1.2	41.60 \pm 0.8	42.78 \pm 0.8	43.52 \pm 1.0	43.82 \pm 0.9
BWT	–	18.5 \pm 0.8	8.06 \pm 1.2	6.77 \pm 1.2	5.97 \pm 0.8	8.25 \pm 0.8	8.03 \pm 0.8	7.12 \pm 0.4	7.16 \pm 0.4	3.46 \pm 0.4	3.25 \pm 0.5
google / Gemma-2B-it											
OP	32.3 \pm 0.2	31.89 \pm 0.8	32.85 \pm 1.4	26.48 \pm 1.5	28.35 \pm 1.6	31.14 \pm 1.2	32.42 \pm 1.0	33.25 \pm 0.9	33.73 \pm 0.8	33.41 \pm 0.9	33.96 \pm 1.0
BWT	–	15.28 \pm 0.4	12.27 \pm 0.9	18.25 \pm 0.9	16.96 \pm 1.2	15.77 \pm 0.7	14.25 \pm 0.5	13.66 \pm 0.5	12.36 \pm 0.4	8.50 \pm 0.5	7.94 \pm 0.8
meta-llama / LLaMA-3-1B-Instruct											
OP	31.16 \pm 0.4	29.73 \pm 1.6	30.12 \pm 2.0	32.19 \pm 2.0	31.96 \pm 1.6	29.38 \pm 1.2	30.76 \pm 1.2	33.73 \pm 1.2	32.94 \pm 0.8	36.14 \pm 0.7	37.46 \pm 0.8
BWT	–	17.03 \pm 1.2	15.2 \pm 1.6	10.74 \pm 1.6	11.62 \pm 1.2	13.57 \pm 0.8	11.34 \pm 0.8	12.36 \pm 0.8	12.89 \pm 1.2	7.36 \pm 0.8	5.11 \pm 0.8



(a) Visualization of Activated Ranks across Layers and Transformer Modules

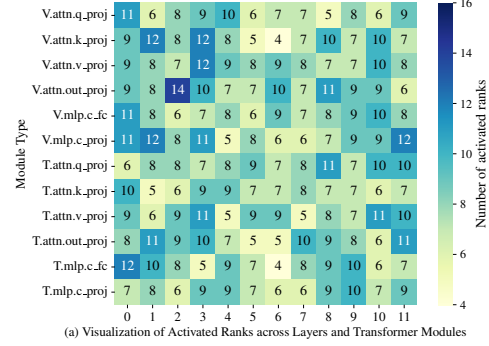


(b) Ratio of Activated Ranks Cumulated over Module Types

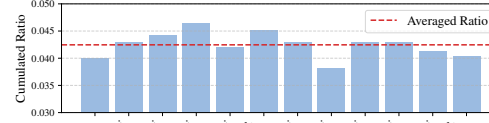


(c) Ratio of Activated Ranks Cumulated over Layers

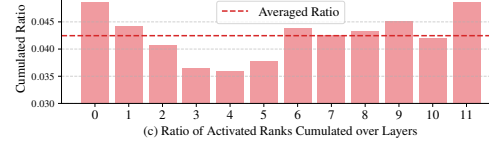
Figure 5: Visualization and statistical analysis of rank activation on the Aircraft dataset.



(a) Visualization of Activated Ranks across Layers and Transformer Modules



(b) Ratio of Activated Ranks Cumulated over Module Types



(c) Ratio of Activated Ranks Cumulated over Layers

Figure 6: Visualization and statistical analysis of rank activation on the Oxford Pets dataset.

Rank allocation analysis. We visualize rank allocation across datasets in Fig. 5 and Fig. 6 (extended in Appendix Fig. 11–18). The results show that CoDyRA adapts the number of active ranks differently across locations and tasks, reflecting the varying demands of each dataset. These strike a balance between plasticity and stability, demonstrating the method’s ability to regulate forgetting while enabling effective task learning.

For **Aircraft**, ranks concentrate in the text encoder’s Attention Output projection (Fig. 5(b)) and deeper layers 6–10 (Fig. 5(c)). In contrast, for **Pets**, allocation shifts to the vision encoder (Attn Value/Output and MLP Projection; Fig. 6(b)), primarily targeting the first and last layers (Fig. 6(c)).

These distinct patterns highlight CoDyRA’s ability to dynamically adjust capacity for effective domain adaptation while preserving existing knowledge. Further analysis is provided in Appendix B.8.

Computation cost. We compare computational costs in terms of trainable parameters and inference overhead, as shown in Table 4. For MoE-Adapter, the gap between training and testing parameters stems from its mixture-of-experts design: all experts are active during training, while only the top-2 are used at inference. RAIL-Primal introduces extra overhead from high-dimensional feature expansion via projection and regression layers. RAIL-Dual further increases memory use by storing image features for all samples across 1,100 classes. These methods all incur linearly growing costs as

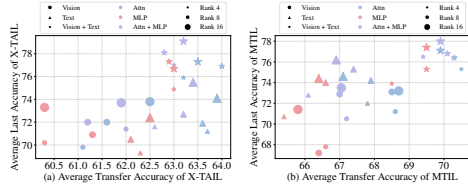


Figure 7: Ablations on different insertion locations and the impact of varying the initial rank.

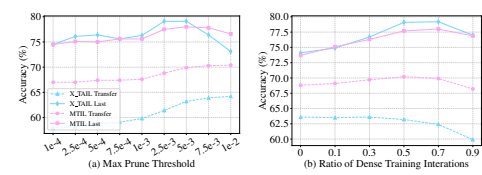


Figure 8: Analyses (a) maximum pruning threshold and (b) ratios of dense training iterations.

tasks increase. In contrast, our method reduces training overhead by retaining only high-importance ranks; once merged into the pre-trained weights, the updates add zero memory cost at inference.

4.3 Ablation Studies

Effects of insertion locations and initial ranks. We study the impact of insertion locations and initial ranks (Fig. 7), consistent with our earlier analyses (Fig. 2). Training restricted to the vision encoder significantly reduces transfer accuracy, indicating degraded pre-trained capabilities. At certain locations, increasing rank improves adaptation but does not always hinder transfer accuracy.

Interestingly, restricting updates to only Attention modules can even surpass our reported state-of-the-art Transfer results (Table 1, Table 5), but at the cost of weaker adaptation. To balance adaptation and retention, we update across all modules by default, achieving an optimal trade-off between learning new tasks and preserving pre-trained knowledge.

Analyses of pruning threshold and dense-iteration ratio. To understand the trade-off between learning and forgetting, we vary the maximum threshold κ_{\max} and the dense training ratio (Fig. 8). Raising κ_{\max} improves Last accuracy by pruning noisy ranks, but overly aggressive pruning limits adaptation. For simplicity, we do not tune the value of κ_{\max} for each downstream task. The dense-iteration ratio controls pruning onset: pruning from the start (ratio = 0) removes ranks before they learn useful knowledge, while delaying too long risks retaining noisy ranks that do not get pruned.

5 Conclusion

We introduced CoDyRA, a dynamic rank-selective framework for continual learning in large pre-trained models, including both CLIP and LLMs. Guided by sparsity-promoting regularization, CoDyRA automatically identifies the ranks needed, keeping updates close to the model’s previous state while preserving essential ranks. This approach eliminates the need for data replay, task identifiers, or complex architectural expansion. Extensive evaluation across diverse benchmarks confirms that CoDyRA achieves superior performance, effectively balancing learning and knowledge retention across modalities and scales.

Future works. CoDyRA updates the model continually by balancing learning and forgetting in the current task. While enabling a flexible and efficient CL process with strong results, future work will further refine modeling of rank relationships, inter-task dependencies, and forgetting measures.

Impact Statement

CoDyRA’s sparse, adaptive, importance-aware low-rank subspace learning significantly reduces compute and memory demands for continual learning, enabling on-device personalization in domains such as mobile health and education and empowering resource-constrained users and organizations. As a fundamental research effort, CodyRA does not address potential biases or hazards in training data, and its incremental updates could introduce privacy risks or stealthy backdoors. We therefore recommend transparent update logging, regular audits, and differential-privacy safeguards. Although more efficient than full fine-tuning, large-scale deployment still incurs energy costs; developers should monitor resource use, leverage low-power hardware, and explore carbon offsets.

Table 4: Computation cost.

Methods	Training Params.	Additional Infer. Params. / Mem.
LWF [38]	129.6M	None
ZSCL [99]	129.6M	None
MoE-Adapters [93]	59.8M	13.35M
RAIL [90]	N/A	24.18M / 9.01M
CoDyRA	4.4M	None

Acknowledgments and Disclosure of Funding

This work was partially supported by the ARC DECRA Fellowship (DE230101591) awarded to D. Gong. H. Lu is affiliated with CSIRO Data61 through a PhD scholarship and acknowledges the support of the Google PhD Fellowship.

References

- [1] R. Aljundi, F. Babiloni, M. Elhoseiny, M. Rohrbach, and T. Tuytelaars. Memory aware synapses: Learning what (not) to forget. In *Proceedings of the European conference on computer vision (ECCV)*, pages 139–154, 2018.
- [2] R. Aljundi, K. Kelchtermans, and T. Tuytelaars. Task-free continual learning. In *Proceedings of the IEEE/CVF Conference on Computer Vision and Pattern Recognition*, pages 11254–11263, 2019.
- [3] R. Aljundi, M. Lin, B. Goujaud, and Y. Bengio. Gradient based sample selection for online continual learning. *Advances in neural information processing systems*, 32, 2019.
- [4] A. Beck and M. Teboulle. A fast iterative shrinkage-thresholding algorithm for linear inverse problems. *SIAM journal on imaging sciences*, 2(1):183–202, 2009.
- [5] D. Biderman, J. Portes, J. J. G. Ortiz, M. Paul, P. Greengard, C. Jennings, D. King, S. Havens, V. Chiley, J. Frankle, et al. Lora learns less and forgets less. *arXiv preprint arXiv:2405.09673*, 2024.
- [6] L. Bossard, M. Guillaumin, and L. Van Gool. Food-101–mining discriminative components with random forests. In *Proceedings of the European conference on computer vision (ECCV)*, pages 446–461, 2014.
- [7] T. Brown, B. Mann, N. Ryder, M. Subbiah, J. D. Kaplan, P. Dhariwal, A. Neelakantan, P. Shyam, G. Sastry, A. Askell, et al. Language models are few-shot learners. *Advances in neural information processing systems*, 33:1877–1901, 2020.
- [8] A. Chaudhry, P. K. Dokania, T. Ajanthan, and P. H. Torr. Riemannian walk for incremental learning: Understanding forgetting and intransigence. In *Proceedings of the European conference on computer vision (ECCV)*, pages 532–547, 2018.
- [9] A. Chaudhry, M. Ranzato, M. Rohrbach, and M. Elhoseiny. Efficient lifelong learning with a-gem. *arXiv preprint arXiv:1812.00420*, 2018.
- [10] M. Cimpoi, S. Maji, I. Kokkinos, S. Mohamed, and A. Vedaldi. Describing textures in the wild. In *Proceedings of the IEEE conference on computer vision and pattern recognition*, pages 3606–3613, 2014.
- [11] M. De Lange, R. Aljundi, M. Masana, S. Parisot, X. Jia, A. Leonardis, G. Slabaugh, and T. Tuytelaars. A continual learning survey: Defying forgetting in classification tasks. *IEEE transactions on pattern analysis and machine intelligence*, 44(7):3366–3385, 2021.
- [12] J. Deng, W. Dong, R. Socher, L.-J. Li, K. Li, and L. Fei-Fei. Imagenet: A large-scale hierarchical image database. In *2009 IEEE conference on computer vision and pattern recognition*, pages 248–255. Ieee, 2009.
- [13] L. Deng. The mnist database of handwritten digit images for machine learning research [best of the web]. *IEEE signal processing magazine*, 29(6):141–142, 2012.
- [14] N. Ding, X. Lv, Q. Wang, Y. Chen, B. Zhou, Z. Liu, and M. Sun. Sparse low-rank adaptation of pre-trained language models. *arXiv preprint arXiv:2311.11696*, 2023.
- [15] Y. Ding, L. Liu, C. Tian, J. Yang, and H. Ding. Don’t stop learning: Towards continual learning for the clip model. *arXiv preprint arXiv:2207.09248*, 2022.
- [16] A. Dubey, A. Jauhri, A. Pandey, A. Kadian, A. Al-Dahle, A. Letman, A. Mathur, A. Schelten, A. Yang, A. Fan, et al. The llama 3 herd of models. *arXiv e-prints*, pages arXiv–2407, 2024.

[17] A. Fang, A. M. Jose, A. Jain, L. Schmidt, A. T. Toshev, and V. Shankar. Data filtering networks. In *The Twelfth International Conference on Learning Representations*, 2024. URL <https://openreview.net/forum?id=KAk6ngZ09F>.

[18] M. Farajtabar, N. Azizan, A. Mott, and A. Li. Orthogonal gradient descent for continual learning. In *International conference on artificial intelligence and statistics*, pages 3762–3773. PMLR, 2020.

[19] L. Fei-Fei, R. Fergus, and P. Perona. Learning generative visual models from few training examples: An incremental bayesian approach tested on 101 object categories. In *2004 conference on computer vision and pattern recognition workshop*, pages 178–178. IEEE, 2004.

[20] Q. Gao, C. Zhao, Y. Sun, T. Xi, G. Zhang, B. Ghanem, and J. Zhang. A unified continual learning framework with general parameter-efficient tuning. In *Proceedings of the IEEE/CVF International Conference on Computer Vision*, pages 11483–11493, 2023.

[21] S. Garg, M. Farajtabar, H. Pouransari, R. Vemulapalli, S. Mehta, O. Tuzel, V. Shankar, and F. Faghri. Tic-clip: Continual training of clip models. *arXiv preprint arXiv:2310.16226*, 2023.

[22] A. R. Gonzales, N. Spring, T. Kew, M. Kostrzewa, A. Säuberli, M. Müller, and S. Ebling. A new dataset and efficient baselines for document-level text simplification in german. In *Proceedings of the Third Workshop on New Frontiers in Summarization*, pages 152–161, 2021.

[23] R. Hadsell, D. Rao, A. A. Rusu, and R. Pascanu. Embracing change: Continual learning in deep neural networks. *Trends in cognitive sciences*, 24(12):1028–1040, 2020.

[24] J. He, Z. Duan, and F. Zhu. Cl-lora: Continual low-rank adaptation for rehearsal-free class-incremental learning. In *Proceedings of the Computer Vision and Pattern Recognition Conference*, pages 30534–30544, 2025.

[25] P. Helber, B. Bischke, A. Dengel, and D. Borth. Eurosat: A novel dataset and deep learning benchmark for land use and land cover classification. *IEEE Journal of Selected Topics in Applied Earth Observations and Remote Sensing*, 12(7):2217–2226, 2019.

[26] D. Hendrycks and K. Gimpel. Gaussian error linear units (gelus). *arXiv preprint arXiv:1606.08415*, 2016.

[27] E. J. Hu, Y. Shen, P. Wallis, Z. Allen-Zhu, Y. Li, S. Wang, L. Wang, and W. Chen. Lora: Low-rank adaptation of large language models. *arXiv preprint arXiv:2106.09685*, 2021.

[28] Y. Hu, T. Ganter, H. Deilamsalehy, F. Dernoncourt, H. Foroosh, and F. Liu. Meetingbank: A benchmark dataset for meeting summarization. In *Proceedings of the 61st Annual Meeting of the Association for Computational Linguistics (Volume 1: Long Papers)*, pages 16409–16423, 2023.

[29] L. Huang, X. Cao, H. Lu, Y. Meng, F. Yang, and X. Liu. Mind the gap: Preserving and compensating for the modality gap in clip-based continual learning. *arXiv preprint arXiv:2507.09118*, 2025.

[30] G. Ilharco, M. Wortsman, R. Wightman, C. Gordon, N. Carlini, R. Taori, A. Dave, V. Shankar, H. Namkoong, J. Miller, H. Hajishirzi, A. Farhadi, and L. Schmidt. Openclip, July 2021. URL <https://doi.org/10.5281/zenodo.5143773>.

[31] S. Jha, D. Gong, H. Zhao, and L. Yao. Npcl: Neural processes for uncertainty-aware continual learning. *arXiv preprint arXiv:2310.19272*, 2023.

[32] S. Jha, D. Gong, and L. Yao. CLAP4CLIP: Continual learning with probabilistic finetuning for vision-language models. In *The Thirty-eighth Annual Conference on Neural Information Processing Systems*, 2024. URL <https://openreview.net/forum?id=rF1YRtZfoJ>.

[33] J. Kirkpatrick, R. Pascanu, N. Rabinowitz, J. Veness, G. Desjardins, A. A. Rusu, K. Milan, J. Quan, T. Ramalho, A. Grabska-Barwinska, et al. Overcoming catastrophic forgetting in neural networks. *Proceedings of the national academy of sciences*, 114(13):3521–3526, 2017.

[34] J. Krause, M. Stark, J. Deng, and L. Fei-Fei. 3d object representations for fine-grained categorization. In *Proceedings of the IEEE international conference on computer vision workshops*, pages 554–561, 2013.

[35] A. Krizhevsky, G. Hinton, et al. Learning multiple layers of features from tiny images. 2009.

[36] C. Li, H. Farkhoor, R. Liu, and J. Yosinski. Measuring the intrinsic dimension of objective landscapes. *arXiv preprint arXiv:1804.08838*, 2018.

[37] J. Li, D. Li, C. Xiong, and S. Hoi. Blip: Bootstrapping language-image pre-training for unified vision-language understanding and generation. In *International conference on machine learning*, pages 12888–12900. PMLR, 2022.

[38] Z. Li and D. Hoiem. Learning without forgetting. *IEEE transactions on pattern analysis and machine intelligence*, 40(12):2935–2947, 2017.

[39] V. W. Liang, Y. Zhang, Y. Kwon, S. Yeung, and J. Y. Zou. Mind the gap: Understanding the modality gap in multi-modal contrastive representation learning. *Advances in Neural Information Processing Systems*, 35:17612–17625, 2022.

[40] Y.-S. Liang and W.-J. Li. Inflora: Interference-free low-rank adaptation for continual learning. In *Proceedings of the IEEE/CVF Conference on Computer Vision and Pattern Recognition*, pages 23638–23647, 2024.

[41] W. Liu, F. Zhu, L. Wei, and Q. Tian. C-clip: Multimodal continual learning for vision-language model. In *The Thirteenth International Conference on Learning Representations*, 2025.

[42] Y. Liu, Y. Su, A.-A. Liu, B. Schiele, and Q. Sun. Mnemonics training: Multi-class incremental learning without forgetting. In *Proceedings of the IEEE/CVF conference on Computer Vision and Pattern Recognition*, pages 12245–12254, 2020.

[43] Z. Liu, J. Lyn, W. Zhu, X. Tian, and Y. Graham. Alora: Allocating low-rank adaptation for fine-tuning large language models. *arXiv preprint arXiv:2403.16187*, 2024.

[44] D. Lopez-Paz and M. Ranzato. Gradient episodic memory for continual learning. *Advances in neural information processing systems*, 30, 2017.

[45] I. Loshchilov and F. Hutter. Decoupled weight decay regularization. *arXiv preprint arXiv:1711.05101*, 2017.

[46] P. Lu, S. Mishra, T. Xia, L. Qiu, K.-W. Chang, S.-C. Zhu, O. Tafjord, P. Clark, and A. Kalyan. Learn to explain: Multimodal reasoning via thought chains for science question answering. *Advances in Neural Information Processing Systems*, 35:2507–2521, 2022.

[47] S. Lu, D. Guo, S. Ren, J. Huang, A. Svyatkovskiy, A. Blanco, C. Clement, D. Drain, D. Jiang, D. Tang, et al. Codexglue: A machine learning benchmark dataset for code understanding and generation. *arXiv preprint arXiv:2102.04664*, 2021.

[48] Z. Luo, Y. Liu, B. Schiele, and Q. Sun. Class-incremental exemplar compression for class-incremental learning. In *Proceedings of the IEEE/CVF Conference on Computer Vision and Pattern Recognition*, pages 11371–11380, 2023.

[49] S. Maji, E. Rahtu, J. Kannala, M. Blaschko, and A. Vedaldi. Fine-grained visual classification of aircraft. *arXiv preprint arXiv:1306.5151*, 2013.

[50] S. Malladi, A. Wettig, D. Yu, D. Chen, and S. Arora. A kernel-based view of language model fine-tuning. In *International Conference on Machine Learning*, pages 23610–23641. PMLR, 2023.

[51] M. McCloskey and N. J. Cohen. Catastrophic interference in connectionist networks: The sequential learning problem. In *Psychology of learning and motivation*, volume 24, pages 109–165. Elsevier, 1989.

[52] M. D. McDonnell, D. Gong, A. Parvaneh, E. Abbasnejad, and A. van den Hengel. Ranpac: Random projections and pre-trained models for continual learning. *Advances in Neural Information Processing Systems*, 36, 2024.

[53] F. Meng, Z. Wang, and M. Zhang. Pissa: Principal singular values and singular vectors adaptation of large language models. *arXiv preprint arXiv:2404.02948*, 2024.

[54] K. Meng, D. Bau, A. Andonian, and Y. Belinkov. Locating and editing factual associations in gpt. *Advances in neural information processing systems*, 35:17359–17372, 2022.

[55] S. Mishra, A. Mitra, N. Varshney, B. Sachdeva, P. Clark, C. Baral, and A. Kalyan. Numglue: A suite of fundamental yet challenging mathematical reasoning tasks. *arXiv preprint arXiv:2204.05660*, 2022.

[56] C. V. Nguyen, A. Achille, M. Lam, T. Hassner, V. Mahadevan, and S. Soatto. Toward understanding catastrophic forgetting in continual learning. *arXiv preprint arXiv:1908.01091*, 2019.

[57] M.-E. Nilsback and A. Zisserman. Automated flower classification over a large number of classes. In *2008 Sixth Indian conference on computer vision, graphics & image processing*, pages 722–729. IEEE, 2008.

[58] O. M. Parkhi, A. Vedaldi, A. Zisserman, and C. Jawahar. Cats and dogs. In *2012 IEEE conference on computer vision and pattern recognition*, pages 3498–3505. IEEE, 2012.

[59] J. Pearl. Direct and indirect effects. In *Probabilistic and causal inference: the works of Judea Pearl*, pages 373–392. 2022.

[60] Y.-Y. Qian, Y.-Z. Xu, Z.-Y. Zhang, P. Zhao, and Z.-H. Zhou. Treelora: Efficient continual learning via layer-wise loras guided by a hierarchical gradient-similarity tree. *arXiv preprint arXiv:2506.10355*, 2025.

[61] F. Qiao and M. Mahdavi. Learn more, but bother less: parameter efficient continual learning. *Advances in Neural Information Processing Systems*, 37:97476–97498, 2024.

[62] A. Radford, J. W. Kim, C. Hallacy, A. Ramesh, G. Goh, S. Agarwal, G. Sastry, A. Askell, P. Mishkin, J. Clark, et al. Learning transferable visual models from natural language supervision. In *International conference on machine learning*, pages 8748–8763. PMLR, 2021.

[63] S.-A. Rebuffi, A. Kolesnikov, G. Sperl, and C. H. Lampert. icarl: Incremental classifier and representation learning. In *Proceedings of the IEEE conference on Computer Vision and Pattern Recognition*, pages 2001–2010, 2017.

[64] S.-A. Rebuffi, A. Kolesnikov, G. Sperl, and C. H. Lampert. icarl: Incremental classifier and representation learning. In *Proceedings of the IEEE conference on Computer Vision and Pattern Recognition*, pages 2001–2010, 2017.

[65] A. Roy, R. Moullick, V. K. Verma, S. Ghosh, and A. Das. Convolutional prompting meets language models for continual learning. In *Proceedings of the IEEE/CVF conference on computer vision and pattern recognition*, pages 23616–23626, 2024.

[66] J. Schulman and T. M. Lab. Lora without regret. *Thinking Machines Lab: Connectionism*, 2025. doi: 10.64434/tml.20250929. <https://thinkingmachines.ai/blog/lora/>.

[67] A. Shah, S. Paturi, and S. Chava. Trillion dollar words: A new financial dataset, task & market analysis. *arXiv preprint arXiv:2305.07972*, 2023.

[68] J. S. Smith, L. Karlinsky, V. Gutta, P. Cascante-Bonilla, D. Kim, A. Arbelle, R. Panda, R. Feris, and Z. Kira. Coda-prompt: Continual decomposed attention-based prompting for rehearsal-free continual learning. In *Proceedings of the IEEE/CVF Conference on Computer Vision and Pattern Recognition*, pages 11909–11919, 2023.

[69] L. Tang, Z. Tian, K. Li, C. He, H. Zhou, H. Zhao, X. Li, and J. Jia. Mind the interference: Retaining pre-trained knowledge in parameter efficient continual learning of vision-language models. In *European Conference on Computer Vision*, pages 346–365. Springer, 2025.

[70] G. Team, T. Mesnard, C. Hardin, R. Dadashi, S. Bhupatiraju, S. Pathak, L. Sifre, M. Rivière, M. S. Kale, J. Love, et al. Gemma: Open models based on gemini research and technology. *arXiv preprint arXiv:2403.08295*, 2024.

[71] R. Tibshirani. Regression shrinkage and selection via the lasso. *Journal of the Royal Statistical Society Series B: Statistical Methodology*, 58(1):267–288, 1996.

[72] H. Touvron, L. Martin, K. Stone, P. Albert, A. Almahairi, Y. Babaei, N. Bashlykov, S. Batra, P. Bhargava, S. Bhosale, et al. Llama 2: Open foundation and fine-tuned chat models. *arXiv preprint arXiv:2307.09288*, 2023.

[73] F.-Y. Wang, D.-W. Zhou, L. Liu, H.-J. Ye, Y. Bian, D.-C. Zhan, and P. Zhao. Beef: Bi-compatible class-incremental learning via energy-based expansion and fusion. In *The Eleventh International Conference on Learning Representations*, 2022.

[74] F.-Y. Wang, D.-W. Zhou, H.-J. Ye, and D.-C. Zhan. Foster: Feature boosting and compression for class-incremental learning. In *European conference on computer vision*, pages 398–414. Springer, 2022.

[75] H. Wang, H. Lu, L. Yao, and D. Gong. Self-expansion of pre-trained models with mixture of adapters for continual learning. *arXiv preprint arXiv:2403.18886*, 2024.

[76] L. Wang, J. Xie, X. Zhang, M. Huang, H. Su, and J. Zhu. Hierarchical decomposition of prompt-based continual learning: Rethinking obscured sub-optimality. *Advances in Neural Information Processing Systems*, 36:69054–69076, 2023.

[77] L. Wang, X. Zhang, H. Su, and J. Zhu. A comprehensive survey of continual learning: Theory, method and application. *IEEE Transactions on Pattern Analysis and Machine Intelligence*, 2024.

[78] L. Wang, J. Xie, X. Zhang, H. Su, and J. Zhu. Hide-pet: continual learning via hierarchical decomposition of parameter-efficient tuning. *IEEE Transactions on Pattern Analysis and Machine Intelligence*, 2025.

[79] R. Wang, X. Duan, G. Kang, J. Liu, S. Lin, S. Xu, J. Lü, and B. Zhang. Attriclip: A non-incremental learner for incremental knowledge learning. In *Proceedings of the IEEE/CVF Conference on Computer Vision and Pattern Recognition*, pages 3654–3663, 2023.

[80] X. Wang, T. Chen, Q. Ge, H. Xia, R. Bao, R. Zheng, Q. Zhang, T. Gui, and X.-J. Huang. Orthogonal subspace learning for language model continual learning. In *Findings of the Association for Computational Linguistics: EMNLP 2023*, pages 10658–10671, 2023.

[81] X. Wang, Y. Zhang, T. Chen, S. Gao, S. Jin, X. Yang, Z. Xi, R. Zheng, Y. Zou, T. Gui, et al. Trace: A comprehensive benchmark for continual learning in large language models. *arXiv preprint arXiv:2310.06762*, 2023.

[82] Y. Wang, Z. Huang, and X. Hong. S-prompts learning with pre-trained transformers: An occam’s razor for domain incremental learning. *Advances in Neural Information Processing Systems*, 35:5682–5695, 2022.

[83] Z. Wang, Z. Zhang, S. Ebrahimi, R. Sun, H. Zhang, C.-Y. Lee, X. Ren, G. Su, V. Perot, J. Dy, et al. Dualprompt: Complementary prompting for rehearsal-free continual learning. In *European Conference on Computer Vision*, pages 631–648. Springer, 2022.

[84] Z. Wang, Z. Zhang, C.-Y. Lee, H. Zhang, R. Sun, X. Ren, G. Su, V. Perot, J. Dy, and T. Pfister. Learning to prompt for continual learning. In *Proceedings of the IEEE/CVF Conference on Computer Vision and Pattern Recognition*, pages 139–149, 2022.

[85] M. Wortsman, G. Ilharco, J. W. Kim, M. Li, S. Kornblith, R. Roelofs, R. G. Lopes, H. Hajishirzi, A. Farhadi, H. Namkoong, et al. Robust fine-tuning of zero-shot models. In *Proceedings of the IEEE/CVF Conference on Computer Vision and Pattern Recognition*, pages 7959–7971, 2022.

[86] T. Wu, J. Wang, Z. Zhao, and N. Wong. Mixture-of-subspaces in low-rank adaptation. *arXiv preprint arXiv:2406.11909*, 2024.

[87] Y. Wu, H. Piao, L.-K. Huang, R. Wang, W. Li, H. Pfister, D. Meng, K. Ma, and Y. Wei. SD-loRA: Scalable decoupled low-rank adaptation for class incremental learning. In *The Thirteenth International Conference on Learning Representations*, 2025. URL <https://openreview.net/forum?id=5U1rlpX68A>.

[88] Z. Wu, A. Arora, Z. Wang, A. Geiger, D. Jurafsky, C. D. Manning, and C. Potts. Reft: Representation finetuning for language models. *Advances in Neural Information Processing Systems*, 37:63908–63962, 2024.

[89] J. Xiao, J. Hays, K. A. Ehinger, A. Oliva, and A. Torralba. Sun database: Large-scale scene recognition from abbey to zoo. In *2010 IEEE computer society conference on computer vision and pattern recognition*, pages 3485–3492. IEEE, 2010.

[90] Y. Xu, Y. Chen, J. Nie, Y. Wang, H. Zhuang, and M. Okumura. Advancing cross-domain discriminability in continual learning of vision-language models. *Advances in Neural Information Processing Systems*, 37:51552–51576, 2024.

[91] Q. Yan, D. Gong, Y. Liu, A. van den Hengel, and J. Q. Shi. Learning bayesian sparse networks with full experience replay for continual learning. In *Proceedings of the IEEE/CVF Conference on Computer Vision and Pattern Recognition*, pages 109–118, 2022.

[92] S. Yan, J. Xie, and X. He. Der: Dynamically expandable representation for class incremental learning. In *Proceedings of the IEEE/CVF Conference on Computer Vision and Pattern Recognition*, pages 3014–3023, 2021.

[93] J. Yu, Y. Zhuge, L. Zhang, P. Hu, D. Wang, H. Lu, and Y. He. Boosting continual learning of vision-language models via mixture-of-experts adapters. In *Proceedings of the IEEE/CVF Conference on Computer Vision and Pattern Recognition*, pages 23219–23230, 2024.

[94] F. Zenke, B. Poole, and S. Ganguli. Continual learning through synaptic intelligence. In *International conference on machine learning*, pages 3987–3995. PMLR, 2017.

[95] J. Zhang, Y. Zhao, D. Chen, X. Tian, H. Zheng, and W. Zhu. Milora: Efficient mixture of low-rank adaptation for large language models fine-tuning. *arXiv preprint arXiv:2410.18035*, 2024.

[96] Q. Zhang, M. Chen, A. Bukharin, N. Karampatziakis, P. He, Y. Cheng, W. Chen, and T. Zhao. Adalora: Adaptive budget allocation for parameter-efficient fine-tuning. *arXiv preprint arXiv:2303.10512*, 2023.

[97] W. Zhang, P. Janson, R. Aljundi, and M. Elhoseiny. Overcoming generic knowledge loss with selective parameter update. In *Proceedings of the IEEE/CVF Conference on Computer Vision and Pattern Recognition*, pages 24046–24056, 2024.

[98] C. Zhao, Y. Li, and C. Caragea. C-stance: A large dataset for chinese zero-shot stance detection. In *Proceedings of the 61st Annual Meeting of the Association for Computational Linguistics (Volume 1: Long Papers)*, pages 13369–13385, 2023.

[99] Z. Zheng, M. Ma, K. Wang, Z. Qin, X. Yue, and Y. You. Preventing zero-shot transfer degradation in continual learning of vision-language models. *arXiv preprint arXiv:2303.06628*, 2023.

[100] B. Zhou, A. Lapedriza, A. Khosla, A. Oliva, and A. Torralba. Places: A 10 million image database for scene recognition. *IEEE transactions on pattern analysis and machine intelligence*, 40(6):1452–1464, 2017.

[101] D.-W. Zhou, Q.-W. Wang, H.-J. Ye, and D.-C. Zhan. A model or 603 exemplars: Towards memory-efficient class-incremental learning. *arXiv preprint arXiv:2205.13218*, 2022.

[102] D.-W. Zhou, Y. Zhang, J. Ning, H.-J. Ye, D.-C. Zhan, and Z. Liu. Learning without forgetting for vision-language models. *arXiv preprint arXiv:2305.19270*, 2023.

[103] D.-W. Zhou, H.-L. Sun, H.-J. Ye, and D.-C. Zhan. Expandable subspace ensemble for pre-trained model-based class-incremental learning. In *Proceedings of the IEEE/CVF Conference on Computer Vision and Pattern Recognition*, pages 23554–23564, 2024.

- [104] K. Zhou, J. Yang, C. C. Loy, and Z. Liu. Conditional prompt learning for vision-language models. In *Proceedings of the IEEE/CVF Conference on Computer Vision and Pattern Recognition*, pages 16816–16825, 2022.
- [105] K. Zhou, J. Yang, C. C. Loy, and Z. Liu. Learning to prompt for vision-language models. *International Journal of Computer Vision*, 130(9):2337–2348, 2022.
- [106] H. Zhu, Y. Zhang, J. Dong, and P. Koniusz. Bilora: Almost-orthogonal parameter spaces for continual learning. In *Proceedings of the Computer Vision and Pattern Recognition Conference*, pages 25613–25622, 2025.

A Additional Details of the Proposed Method

In Sec. 3.3 of the main paper, we introduce our method for learning dynamic rank-selective parameter updates to pre-trained weight matrices. We leverage a learnable vector to represent the importance of each rank, which is updated through a soft-thresholding operation. In this section, we provide more details to enhance clarity and understanding.

A.1 Full Derivation of Eq. (4)

For simplicity, we omit the notation for the training task t in the following derivations. With a slight abuse of notation, we use subscript t to represent t -th training iteration. At the t -th training iteration, the training loss with ℓ_1 sparse regularization, as defined in the main paper, is:

$$\mathcal{L}_{\text{train}}(\Delta_t) := \mathcal{L}_{\text{sup}}(\Delta_t) + \lambda \sum_{m=1}^M \|\mathbf{w}_t^m\|_1, \quad (3)$$

where \mathcal{L}_{sup} is the supervised training loss, Δ_t is the all trainable parameters $\{\mathbf{w}_t^m, \mathbf{B}_t^m, \mathbf{A}_t^m\}_{m=1}^M$ at t -th iteration, M is the total number of pre-trained weight matrices with LoRA of rank r , \mathbf{w}_t^m represents the importance weights of the m -th LoRA module, and $\lambda > 0$ controls the strength of the ℓ_1 regularization.

We apply proximal gradient descent [4] to handle the non-differentiable ℓ_1 regularization of the importance weights [14]. At the t -th iteration, the update rule for the importance weights of each LoRA becomes:

$$\begin{aligned} \mathbf{w}_{t+1}^m &\leftarrow \arg \min_{\mathbf{w}^m} \eta_t \cdot \lambda \|\mathbf{w}^m\|_1 \\ &\quad + \frac{1}{2} \|\mathbf{w}^m - (\mathbf{w}_t^m - \eta_t \nabla_{\mathbf{w}^m} \mathcal{L}_{\text{sup}}(\Delta_t))\|_2^2, \end{aligned} \quad (5)$$

where $\eta_t > 0$ is the step-size of t -th iteration, and $\nabla_{\mathbf{w}^m} \mathcal{L}_{\text{sup}}(\Delta_t)$ is the gradient of the supervised loss with respect to \mathbf{w}^m . This update balances the ℓ_1 sparsity regularization term $\|\mathbf{w}^m\|_1$, with the quadratic penalty term $\frac{1}{2} \|\mathbf{w}^m - \hat{\mathbf{w}}_t^m\|_2^2$, which ensures proximity to the gradient update if importance weights $\hat{\mathbf{w}}_t^m := \mathbf{w}_t^m - \eta_t \nabla_{\mathbf{w}^m} \mathcal{L}_{\text{sup}}(\Delta_t)$. This can be achieved through a soft-thresholding operator \mathcal{T} :

$$\mathbf{w}_{t+1}^m \leftarrow \mathcal{T}_{\eta_t \cdot \lambda}(\mathbf{w}_t^m - \eta_t \nabla_{\mathbf{w}^m} \mathcal{L}_{\text{sup}}(\Delta_t)), \quad (6)$$

where the soft-thresholding operator \mathcal{T} is defined as:

$$\mathcal{T}_\kappa(x) = \mathbb{1}(|x| > \kappa) \cdot (x - \text{sign}(x) \cdot \kappa), \quad (7)$$

such that the input to the operator \mathcal{T}_κ is the elements in $\hat{\mathbf{w}}_t^m$, $\hat{\mathbf{w}}_t^m$ is the value of \mathbf{w}_t^m after the gradient update using only $\mathcal{L}_{\text{sup}}(\Delta_t)$, and $\kappa = \eta_t \cdot \lambda$ is the threshold. The indicator function $\mathbb{1}(\cdot)$ returns 1 if the condition is met, and 0 otherwise, while $\text{sign}(\cdot)$ denotes the sign (+/−) of the input. This concludes our derivation of the dynamic update for the importance weights as presented in the main paper Eq. (4).

A.2 More Discussions on Analytical Results of Sec. 3.2

A.2.1 Takeaway 1 - On Applying LoRA to All Modules

The original LoRA paper applies LoRA only to selected modules (mainly the attention components). Many subsequent LoRA and LoRA-based continual learning works (e.g., InfoLoRA, MoE-Adapters, O-LoRA, etc.) also apply LoRA to only part of the Transformer modules, though the specific choices vary. To clarify this design space, we conducted an analysis to determine which module configuration is most effective. Our results show that applying LoRA to all layers yields clear benefits.

While the theoretical analysis of standard Transformers and full LoRA training dynamics is complex, the empirical Neural Tangent Kernel (eNTK) [50] offers a practical framework for theoretical investigation. The necessity of applying LoRA to all layers, rather than just attention modules, can be explained through the lens of the eNTK.

The eNTK of LoRA approximates that of Full Fine-Tuning (FullFT) only when LoRA is applied to the layers that contain the majority of the parameters. Since the kernel is based on the dot

products of gradients ($K(i, j) = g_i \cdot g_j$), layers with more parameters (e.g., MLPs) typically exert the most influence on the kernel. Restricting updates to attention layers limits the model's ability to approximate the learning dynamics of FullIFT, resulting in "slower learning" or reduced plasticity.

A.2.2 Takeaway 2 - On the Rank-Dependent Plasticity-Stability Balance

We formalize the causality of this balance by defining the trade-off as an informational dilemma rooted in the subspace dimensionality:

High Rank → High Plasticity / Low Stability. The rank (r) dictates the intrinsic dimensionality (degrees of freedom) of the update subspace ΔW . A high rank maximizes the informational capacity of the parameter shift. In the NTK context, maximizing rank pushes the update closer to the FullIFT regime. While this allows for rapid acquisition of new task knowledge (High Plasticity), the larger informational perturbation maximizes disruption to the pre-trained knowledge manifold, leading to catastrophic forgetting (Low Stability).

Low Rank → High Stability / Low Plasticity. Conversely, restricting rank constrains the degrees of freedom. This forces the model to encode only the minimal, essential information for the new task. This minimization of total informational perturbation ensures the model remains informationally proximal to its previous state—a necessary condition for stability.

A lower rank r of the LoRA implies a smaller dimension for the update ΔW . A low rank acts as a structural regularizer. It forces the update to be the "simplest" change necessary to solve the current task. This minimizes the norm $\|\Delta W\|_F$ and reduces the probability that the update vector on the critical subspace of previous tasks.

A.2.3 Takeaway 3 - On the Necessity of Adaptive Optimization

The need for adaptive rank selection stems from the functional variance of model components and the different information requirements of tasks.

Following the theory on intrinsic dimension of objective landscapes [36], different tasks require different degrees of freedom to be solved. And, not all layers contribute equally to the objectives. Adaptivity allows the model to allocate higher ranks to layers with high gradient influence (e.g., specific MLPs) while enforcing sparsity on less critical layers.

A.3 Connections Between Rank Minimizing and Forgetting

As shown in Eq. (2) and (3), we minimize the rank number to regularize the updating strength $\|\Delta \mathbf{W}^{t,m}\|$, $R(\Delta \mathbf{W}^{t,m})$. Minimizing $\|\mathbf{w}^{t,m}\|_1$ with a small rank number encourages minimizing of $\|\Delta \mathbf{W}^{t,m}\|_F$ if given $\mathbf{A}^{t,m}$ and $\mathbf{B}^{t,m}$ (according to Eq. (2)). It limits the update $\Delta \mathbf{W}^{t,m}$ to the minimal dimension necessary. It softly reduces capacity in updates conflicting with critical information encoded in the learned parameters, without introducing additional assumptions.

Another line of work regularizes updates (e.g., LoRA weights or gradients) to lie in subspaces orthogonal to existing parameters [40, 80]. Orthogonal-regularization methods and CoDyRA both aim to mitigate interference, but adopt different strategies with distinct trade-offs, which can be summarized along three aspects.

(1) Orthogonal regularization models and aims to constrain updates to lie in subspaces orthogonal to previous parameters, which effectively reduces interference but also limits the ability to acquire new knowledge. This rigid geometric constraint may suppresses learning new knowledge, and thus is typically softened or relaxed in practice. In contrast, CoDyRA regularizes update simplicity (via rank sparsity) rather than geometry, allowing alignment with prior knowledge when beneficial while keeping updates compact to avoid unintended overwriting. Both of them aims to alleviate interference (for stability) but have trade-off for learning new tasks (for plasticity).

(2) Explicit orthogonal-regularization methods typically require storing the information of already the learned subspace (e.g., projection matrices or singular vectors) to compute orthogonality losses, introducing additional memory overhead and dependence on past task statistics. In contrast, CoDyRA mitigates interference implicitly through sparsity over rank importance. This strictly local objective requires no access to previous tasks, aligning with our goal of natural, memory-free PTM updates.

(3) Standard orthogonal methods typically assume a fixed rank and focus on rotating it. When this rank exceeds a task’s intrinsic dimensionality, the extra dimensions behave as noise, causing unnecessary weight drift. CoDyRA actively prunes such dimensions: a rank pruned to zero induces, by definition, “zero interference” with previous tasks. This yields “zero overlap” for irrelevant dimensions while preserving flexible updates for task-relevant ones.

By mitigating forgetting through different mechanisms and trade-offs, CoDyRA and orthogonal-based methods are complementary. For example, the task-relevant ranks selected by CoDyRA (with nonzero $w^{t,m}$) can be further regularized using orthogonal constraints.

B More Experiments

B.1 Further Details of Experiments.

Details of CLIP CL experiment settings. The MTIL setting consists of 1,201 classes drawn from 11 diverse datasets: Aircraft [49], Caltech101 [19], CIFAR100 [35], DTD [10], EuroSAT [25], Flowers [57], Food [6], MNIST [13], OxfordPet [58], Cars [34], and SUN397 [89]. In the X-TAIL setting, a total of 10 datasets are used, with CIFAR100 [19] excluded to prevent domain overlap, following the protocol in [90]. In line with [90], we evaluate MTIL under both 5-shot and full-shot settings, while X-TAIL is evaluated using a 16-shot setting.

Details of LLM CL experiment settings. We adopt the TRACE benchmark [81], designed for evaluating continual learning in LLMs such as LLaMA [16, 72] and Gemma [70]. TRACE comprises eight diverse datasets standardized into a unified format, spanning domain-specific understanding, multilingual processing, code generation, and mathematical reasoning. Specifically, the tasks are: C-STANKE [98], FOMC [67], MeetingBank [28], Py150 [47], ScienceQA [46], NumGLUE-cm [55], NumGLUE-ds [55], and 20Minuten [22]. In our setup, each task contributes 5,000 training instances and 2,000 testing instances, totaling 40,000 training and 16,000 testing samples.

Given this diversity, we employ task-specific metrics to capture performance nuances: Accuracy is used for classification and reasoning tasks (C-STANKE, FOMC, ScienceQA, NumGLUE); ROUGE-L for summarization (MeetingBank); SARI for multilingual text simplification (20Minuten); and a similarity score for code generation (Py150).

B.2 Evaluation Metrics

To strictly evaluate the plasticity and stability of our method, we employ the following metrics. Let N denote the total number of learned tasks, and $A_{i,j}$ denote the performance (e.g., accuracy, ROUGE, or similarity score) on task j after training on task i .

CLIP Continual Learning Metrics. For the CLIP experiments (MTIL and X-TAIL), we report the following metrics as in [90, 93, 99]:

- **Transfer Accuracy (Transfer):** indicates the model’s zero-shot performance on future domains before they are learned, measures the extent to which the pre-trained zero-shot ability is preserved (or improved) throughout incremental learning.
- **Average Accuracy (Average):** indicates the average accuracy of all learning steps across all domains. It captures the comprehensive performance stability throughout the entire incremental training process.
- **Last Accuracy (Last):** represent the model’s performance on all seen domains after the training is fully completed.

LLM Continual Learning Metrics. For the TRACE benchmark, we adopt the standard metrics as in [81]:

- **Overall Performance (OP):** The average performance across all learned tasks at the end of training.

$$OP = \frac{1}{N} \sum_{j=1}^N A_{N,j}, \quad (8)$$

where $A_{i,j}$ represents the performance on task j after learning task i .

- **Backward Transfer (BWT):** Measures the average performance degradation (forgetting) of previous tasks $j < N$ after learning new tasks. A lower BWT indicates less forgetting (better stability).

$$\text{BWT} = \frac{1}{N-1} \sum_{j=1}^{N-1} (A_{j,j} - A_{N,j}). \quad (9)$$

B.3 Implementation Details.

CLIP experiments. Following established protocols [90, 93, 99], we employ the CLIP ViT-B/16 backbone [62]. CoDyRA is applied to all pre-trained weight matrices in both vision and text encoders, initialized with a rank of 16. CoDyRA is optimized for 500 iterations per task using AdamW [45], with dense training ratios of 0.5 for X-TAIL and 0.7 for MTIL, setting $\kappa_{\max} = 0.005$.

LLM experiments. We adhere to the variable epoch schedule of prior work [60] ($\{2, 1, 3, 2, 1, 2, 2, 3\}$ epochs). We use an initial rank of 16, a dense training ratio of 0.5, and set $\kappa_{\max} = 0.005$. Optimization employs a learning rate of 1×10^{-4} and a batch size of 4. Training utilizes DeepSpeed ZeRO-2 with BF16 mixed-precision and a maximum context length of 1024 tokens. All experiments were conducted on a cluster of four Nvidia H100 GPUs.

B.4 More Experiment Results

B.4.1 Cross-domain task-agnostic incremental learning.

Table 5 presents results on the X-TAIL benchmark [90], a more challenging setting where inference is performed over a mixed label space across all domains. CoDyRA outperforms prior methods across all metrics without requiring auxiliary components, surpassing the zero-shot upper bound in transfer accuracy.

B.4.2 Comparison to fixed-rank LoRA baselines.

Table 6 reports results for fixed-rank LoRA ($r = 4, 8, 16$) and the LoRA variants, including LAE [20], TreeLoRA [60], InfLoRA [40] and CL-LoRA [24]. Several key observations emerge: (1) As LoRA rank increases, Last accuracy improves while Average accuracy declines, aligning with Fig. 2: a relatively higher-rank LoRA facilitates learning new tasks but tends to increase forgetting, while lower-rank LoRA mitigates forgetting but limits adaptation. (2) Fixed-rank LoRA shows a substantial Last-accuracy gap compared to our adaptive method. This suggests that without dynamic rank selection, low-relevance ranks (potentially encoding noise) are retained in the model, impairing generalization to unseen domains and accumulating inter-task interference over time, resulting in severe performance drop. (3) Leveraging fast online LoRA updates, slow EMA aggregation in offline LoRA, and energy-based logit ensembling, LAE substantially outperforms fixed-rank LoRA ($r = 16$). Nonetheless, unlike our method, fixed-rank LoRA lacks fine-grained control over the contribution of individual ranks within each module.

B.4.3 Additional results on full-shot MTIL.

To further extend our evaluation, we report full-shot results on the MTIL benchmark (Table 7). For fairness, we adopt the same domain-prediction design used in recent methods. Consistent with Tables 5 and 1, CoDyRA achieves state-of-the-art performance, surpassing all baselines on both Transfer (unseen-domain generalization) and Last (continual downstream learning).

Table 7 also compares against prompt-based approaches (L2P [84], DualPrompt [83], S-Prompt [82]). Although these methods mitigate task forgetting via key-value matching for prompt selection, they neglect the preservation of pre-trained capabilities—evidenced by substantial drops in transfer accuracy—and further underperform recent domain-prediction approaches on last accuracy.

Table 5: Comparisons on X-TAIL for each domain. The **best** and the **second best** results are highlighted in **red** and **blue**, respectively. Methods marked with \dagger indicate the use of domain prediction or distribution detection [90, 93].

Method	Aircraft	Caltech101	DTD	EuroSAT	Flowers	Food	MNIST	OxfordPet	Cars	SUN397	Average
<i>CLIP</i>											
Zero-shot	23.5	76.8	37.3	36.7	63.6	84.0	46.7	86.7	66.1	63.7	58.5
<i>Transfer</i>											
Zero-shot [62]	–	76.8	37.3	36.7	63.6	84.0	46.7	86.7	66.1	63.7	62.4
LwF [38]	–	66.6	26.9	19.5	51.0	78.4	26.6	68.9	35.5	56.1	47.7
WiSE-FT [85]	–	70.1	31.9	25.3	56.3	79.8	29.9	74.9	45.6	56.8	52.3
iCaRL [64]	–	71.7	35.0	43.0	63.4	86.9	43.9	87.8	63.7	60.0	61.7
ZSCL [99]	–	73.3	32.6	36.8	62.1	83.8	42.1	83.6	56.5	60.2	59.0
MoE-Adapter \dagger [93]	–	71.0	34.9	19.2	63.0	86.6	20.0	87.2	63.7	58.6	56.0
RAIL-Primal \dagger [90]	–	76.8	37.3	36.7	63.6	84.0	46.7	86.7	66.1	63.7	62.4
CoDyRA	–	74.3	36.8	44.2	69.9	83.5	42.8	88.9	64.6	63.4	63.2
CoDyRA \dagger	–	74.3	36.8	44.2	69.9	83.5	42.8	88.9	64.6	63.4	63.2
<i>Average</i>											
LwF [38]	24.7	79.7	38.3	36.9	63.9	81.0	36.5	71.9	42.7	56.7	53.2
WiSE-FT [85]	27.1	76.5	40.9	31.3	68.7	81.6	31.4	74.7	51.7	58.4	54.2
iCaRL [64]	25.4	72.1	37.5	51.6	65.1	87.1	59.1	88.0	63.7	60.1	61.0
ZSCL [99]	36.0	75.0	40.7	40.5	71.0	85.3	46.3	83.3	60.7	61.5	60.0
MoE-Adapter \dagger [93]	43.6	77.9	52.1	34.7	75.9	86.3	45.2	87.4	66.6	60.2	63.0
RAIL-Primal \dagger [90]	42.4	89.8	55.7	68.5	84.0	83.3	65.3	85.8	67.9	64.5	70.7
CoDyRA	41.4	81.0	58.7	77.8	83.4	84.6	64.5	90.4	67.2	64.4	71.3
CoDyRA \dagger	43.9	81.6	60.6	78.4	84.0	84.9	64.6	90.5	67.4	64.4	72.0
<i>Last</i>											
LwF [38]	25.5	72.1	38.9	55.4	65.5	87.3	81.9	88.6	63.6	61.5	64.0
WiSE-FT [85]	21.8	76.8	42.9	20.8	77.5	84.9	30.7	76.6	75.8	72.5	58.0
iCaRL [64]	25.5	72.1	38.9	55.4	65.5	87.3	81.9	88.6	63.6	61.5	64.0
ZSCL [99]	33.1	75.3	43.5	35.2	74.6	87.4	50.4	84.2	77.3	73.4	63.4
MoE-Adapter \dagger [93]	43.2	78.7	57.6	32.8	79.4	86.0	86.7	87.8	78.2	74.2	70.5
RAIL-Primal \dagger [90]	41.7	94.0	66.0	86.4	97.2	82.4	93.1	83.6	75.0	71.3	79.1
CoDyRA	37.7	81.5	65.1	89.9	91.4	85.5	96.8	93.3	77.3	73.5	79.2
CoDyRA \dagger	43.9	82.4	66.6	93.0	93.3	86.3	97.2	94.0	78.5	73.5	80.9

B.4.4 Training stability.

Table 8 reports the mean and standard deviation of CoDyRA’s results in Table 5, averaged over three independent runs. The consistently low variance across metrics demonstrates that our method is stable to random initialization, highlighting CoDyRA’s robust adaptive rank selection.

B.4.5 Analysis in forgetting

We provide a dedicated forgetting analysis in Table 9, quantifying forgetting via Backward Transfer (BWT). It reports BWT of CoDyRA and some relevant CL methods with representation updating. Fixed-rank LoRA serves as a baseline and exhibits significant forgetting due to unconstrained updates without regularization. ZSCL relies on the replay of reference data to help mitigate forgetting. MoE-Adapters isolates task-wise knowledge within specific adapters and adopts domain prediction to further reduce interference. InfLoRA constrains parameter updates to a direction orthogonal to prior tasks to reduce interference. CoDyRA effectively mitigates forgetting by minimizing the rank of updates via sparsity regularization. This ensures the model learns effectively while remaining close to its original state, demonstrating strong retention capabilities with a BWT of only 1.87%.

Moreover, in Table 2, we validate our method in the language domain. The low BWT scores observed in this setting further support our claims of reduced forgetting across architectures.

B.5 Effects of Additional Adaptive Prediction Head on Visual Representations

The related continual learning methods focus on updating the representation with the backbone model (*e.g.*, [84, 93, 99], and CoDyRA) or newly added representation alignment or prediction head [52, 90]. These two types of methods can be seen as orthogonal. We study how the representation updated by the proposed can work with the additional adaptive prediction head, relying on the aggression-based adapters in [90].

Table 6: Extended results for Table 5 on X-TAIL for each domain, comparing continual fine-tuning with different LoRA settings and other LoRA variants.

Method	Aircraft	Caltech101	DTD	EuroSAT	Flowers	Food	MNIST	OxfordPet	Cars	SUN397	Average
<i>CLIP</i>											
Zero-shot	23.5	76.8	37.3	36.7	63.6	84.0	46.7	86.7	66.1	63.7	58.5
<i>Transfer</i>											
Zero-shot [62]	—	76.8	37.3	36.7	63.6	84.0	46.7	86.7	66.1	63.7	62.4
LoRA ($r=4$)	—	74.9	39.4	41.8	67.7	83.3	44.1	87.1	64.2	62.7	62.8
LoRA ($r=8$)	—	77	38.2	38.4	67.8	83.3	44.6	87.6	64	62.8	62.6
LoRA ($r=16$)	—	76.4	39.1	37.5	65.9	82.7	41.9	86.9	63.4	62.7	61.8
LAE-LoRA [20]	—	76.2	39.9	43.8	66.5	83.3	42.7	87.5	63	62.9	62.9
TreeLoRA [60]	—	76.0	36.3	34.0	58.5	77.2	43.3	82.2	49.8	55.8	57.0
InfoLoRA [40]	—	75.8	34.5	29.2	58.1	73.4	38.6	79.5	47.7	50.3	54.1
CL-LoRA [24]	—	73.3	33.7	29.5	58.5	80.3	43.1	85.5	61.5	59.2	58.3
CoDyRA	—	74.3	36.8	44.2	69.9	83.5	42.8	88.9	64.6	63.4	63.2
CoDyRA \dagger	—	74.3	36.8	44.2	69.9	83.5	42.8	88.9	64.6	63.4	63.2
<i>Average</i>											
LoRA ($r=4$)	23.5	78.4	40.6	47.3	71.4	83.7	50.1	87.5	65.1	64	61.2
LoRA ($r=8$)	23.7	78.1	39.7	46.6	71.3	83.7	50.7	87.8	65.4	64.1	61.1
LoRA ($r=16$)	23.6	78.5	40.5	43.0	70.4	82.8	49.5	87.5	64.9	64.0	60.5
LAE-LoRA [20]	29.2	81.3	50.7	68.8	77.4	83.8	53.2	88.5	66.3	64.2	66.4
TreeLoRA [60]	19.3	81.4	55.3	63.9	77.6	80.4	64.3	85.0	54.8	57.6	64.0
InfoLoRA [40]	38.3	84.2	60.1	45.8	79.0	77.5	61.8	82.8	52.2	52.2	63.4
CL-LoRA [24]	39.7	79.2	56.7	58.5	79.1	81.1	64.0	78.0	63.6	60.6	66.0
CoDyRA	41.4	81.0	58.7	77.8	83.4	84.6	64.5	90.4	67.2	64.4	71.3
CoDyRA \dagger	43.9	81.6	60.6	78.4	84.0	84.9	64.6	90.5	67.4	64.4	72.0
<i>Last</i>											
LoRA ($r=4$)	9.75	79.5	40.7	37.5	65.1	82.6	47.1	84.1	57.5	76.3	58
LoRA ($r=8$)	12.7	78.7	39.6	42.6	62.4	82.3	46.8	83.6	60.2	76.1	58.5
LoRA ($r=16$)	13.7	78.6	40.3	39.4	66.1	82.7	50.9	85.7	60.3	76.1	59.4
LAE-LoRA [20]	25.6	81.5	50.2	73.2	79.5	85	70.4	91.1	72.9	75.7	70.5
TreeLoRA [60]	16.0	79.1	59.2	62.3	83.0	83.6	95.0	89.9	71.9	74.2	71.4
InfoLoRA [40]	38.3	85.2	66.6	52.9	92.9	81.6	96.6	90.4	70.1	69.3	74.4
CL-LoRA [24]	39.7	79.8	62.5	70.9	92.9	81.9	95.2	90.5	72.4	73.1	75.9
CoDyRA	37.7	81.5	65.1	89.9	91.4	85.5	96.8	93.3	77.3	73.5	79.2
CoDyRA \dagger	43.9	82.4	66.6	93.0	93.3	86.3	97.2	94.0	78.5	73.5	80.9

We provide a more detailed analysis of the effects of the additional prediction head on the visual representations in X-TAIL setting in Table 10. Note that the Dual version of RAIL [90] stores all visual representations of all samples for all seen classes and domains in memory, it is not included in Tables 5 and 1 for a fair comparison.

RAIL is a regression-based method that applies an additional prediction head on top of the visual representations extracted by the frozen pre-trained vision encoder of the CLIP model. This approach is fully orthogonal to our method, as our focus is on continually incorporating new knowledge into the pre-trained model through dynamic low-rank parameter updates, and we can seamlessly integrate their techniques into our method. Because RAIL heavily relies on the frozen pre-trained model, the Transfer accuracy is limited by the zero-shot performance of the pre-trained model. In contrast, our approach gradually accumulates knowledge into the pre-trained model, enhancing its capability on unseen data and achieving improved Transfer accuracy. Moreover, by leveraging our continually enhanced pre-trained model, coupling our method with RAIL significantly outperforms the original RAIL, which uses a frozen pre-trained model, on the Average and Last metrics.

B.6 Analysis of Changes/Interference w.r.t. Pre-Trained Weights

In Sec. 4.2 of the main paper, Fig. 5 and Fig. 6 visualize and analyze the dynamic ranks assigned to each module. Here, we extend the analysis by comparing parameter changes to pre-trained weights using the amplification factor as in [27]. The amplification factor is given by:

$$\text{Amp} = \frac{\|\Delta \mathbf{W}\|_F}{\|\mathbf{U}^T \mathbf{W} \mathbf{V}^T\|_F}, \quad (10)$$

where \mathbf{W} is the pre-trained weight matrix, and $\Delta \mathbf{W}$ is the parameter change introduced by LoRA. For vanilla LoRA and CoDyRA, $\Delta \mathbf{W}$ is computed using Eq. (1) and Eq. (2), respectively. \mathbf{U} and

Table 7: Comparisons on full-shot MTIL setting.

Method	Aircraft	Caltech101	CIFAR100	DTD	EuroSAT	Flowers	Food	MNIST	OxfordPet	Cars	SUN397	Average
CLIP												
Zero-shot [62]	24.3	88.4	68.2	44.6	54.9	71	88.5	59.4	89	64.7	65.2	65.2
<i>Transfer</i>												
Zero-shot [62]	—	74.5	56.9	39.1	51.1	52.6	72.8	60.6	75.1	30.3	55.9	56.9
LwF [38]	—	56.6	44.6	32.7	39.3	46.6	68.0	46.0	77.4	31.9	60.5	50.4
iCaRL [63]	—	77.1	61.0	40.5	45.3	54.4	74.6	47.9	76.7	36.3	58.6	57.2
LwF-VR [15]	—	73.5	55.6	35.6	41.5	47.0	68.3	53.9	69.3	26.8	51.9	52.3
WiSE-FT [85]	—	86.0	67.4	45.4	50.4	69.1	87.6	61.8	86.8	60.1	66.8	68.1
ZSCL [99]	—	55.7	50.9	30.4	41.4	49.3	71.8	36.3	77.5	55.3	53.4	53.2
L2P \dagger [84]	—	55.7	50.9	30.4	41.4	49.3	71.8	36.3	77.5	55.3	53.4	53.2
DualPrompt \dagger [83]	—	66.7	51.4	28.7	33.7	45.6	70.9	59.5	77.7	49.5	50.4	52.4
S-Prompts \dagger [82]	—	67.3	49.4	26.4	39.7	47.1	70.2	34.3	78.9	56.7	52.2	52.2
DIKI \dagger [69]	—	92.9	69.0	43.2	48.2	67.4	85.2	63.0	87.9	63.8	66.2	68.7
MoE-Adapter \dagger [93]	—	87.9	68.2	44.4	49.9	70.7	88.7	59.7	89.1	64.5	65.5	68.9
CoDyRA \dagger	—	92.4	68.8	45.2	50	69.4	84.2	62.3	88.8	64.6	65	69.1
<i>Average</i>												
LwF [38]	36.3	86.9	72.0	59.0	73.7	60.0	73.6	74.8	80.0	37.3	58.1	64.7
iCaRL [63]	35.5	89.2	72.2	60.6	68.8	70.0	78.2	62.3	81.8	41.2	62.5	65.7
LwF-VR [15]	29.6	87.7	74.4	59.5	72.4	63.6	77.0	66.7	81.2	43.7	60.7	65.1
WiSE-FT [85]	26.7	86.5	64.4	57.1	65.7	58.7	71.1	70.5	75.8	36.9	54.6	60.7
ZSCL [99]	45.1	92.0	80.1	64.3	79.5	81.6	89.6	75.2	88.9	64.7	68.0	75.4
L2P \dagger [84]	38.0	85.2	78.2	61.3	72.9	74.9	79.7	59.1	82.0	59.7	55.4	67.9
DualPrompt \dagger [83]	37.8	84.3	78.5	60.1	71.1	73.2	79.1	73.9	82.3	55.1	52.8	68.0
S-Prompts \dagger [82]	37.5	92.5	77.5	58.2	76.4	74.1	78.8	57.9	83.0	60.8	54.4	68.3
DIKI \dagger [69]	45.1	95.5	83.1	64.8	79.9	83.5	87.0	76.2	89.6	67.0	67.1	76.3
MoE-Adapter \dagger [93]	50.2	91.9	83.1	69.4	78.9	84.0	89.1	73.7	89.3	67.7	66.9	76.7
CoDyRA \dagger	48.3	96.4	83.2	69.1	80.0	84.0	86.0	75.6	90.5	67.5	66.3	77.0
<i>Last</i>												
LwF [38]	26.3	87.5	71.9	66.6	79.9	66.9	83.8	99.6	92.1	66.1	80.4	74.6
iCaRL [63]	35.8	93.0	77.0	70.2	83.3	88.5	90.4	86.7	93.2	81.2	81.9	80.1
LwF-VR [15]	20.5	89.8	72.3	67.6	85.5	73.8	85.7	99.6	93.1	73.3	80.9	76.6
WiSE-FT [85]	27.2	90.8	68.0	68.9	86.9	74.0	87.6	99.6	92.6	77.8	81.3	77.7
ZSCL [99]	40.6	92.2	81.3	70.5	94.8	90.5	91.9	98.7	93.9	85.3	80.2	83.6
L2P \dagger [84]	38.0	87.1	84.2	72.9	86.0	96.1	89.2	99.0	94.1	79.6	76.0	82.0
DualPrompt \dagger [83]	37.8	87.1	84.6	71.8	89.2	96.3	89.1	99.1	94.5	79.9	76.5	82.3
S-Prompts \dagger [82]	37.5	95.1	83.7	70.2	97.5	96.5	89.0	99.1	94.0	79.5	75.8	83.4
DIKI \dagger [69]	45.2	95.7	86.3	72.9	98.0	97.0	89.2	99.4	94.2	81.6	76.6	85.1
MoE-Adapter \dagger [93]	49.8	92.2	86.1	78.1	95.7	94.3	89.5	98.1	89.9	81.6	80.0	85.0
CoDyRA \dagger	48.3	96.8	85.9	77.8	97.5	96.2	88.3	99.0	94.9	80.6	78.6	85.8

Table 8: Statistical significance of CoDyRA results corresponding to Table 5.

	Aircraft	Caltech101	DTD	EuroSAT	Flowers	Food	MNIST	OxfordPet	Cars	SUN397	Average
CoDyRA <i>Transfer</i>	—	74.3 ± 0.52	36.8 ± 0.23	44.2 ± 0.56	69.9 ± 0.56	83.5 ± 0.23	42.8 ± 0.18	88.9 ± 0.42	64.6 ± 0.47	63.4 ± 0.56	63.2 ± 0.28
CoDyRA <i>Average</i>		41.4 ± 0.28	81 ± 0.38	58.7 ± 0.26	77.8 ± 0.47	83.4 ± 0.39	84.6 ± 0.28	64.5 ± 0.14	90.4 ± 0.4	67.2 ± 0.23	64.4 ± 0.47
CoDyRA <i>Last</i>		37.7 ± 0.42	81.5 ± 0.24	65.1 ± 0.63	89.9 ± 0.55	91.4 ± 0.38	85.5 ± 0.16	96.8 ± 0.08	93.3 ± 0.3	77.3 ± 0.66	73.5 ± 0.21

\mathbf{V} represent the top r singular vectors of $\text{SVD}(\Delta\mathbf{W})$, where r is the number of interested ranks in analysis.

A higher amplification factor indicates that low-rank parameter updates amplify directions less emphasized in the pre-trained weights [27]. We visualize the amplification factors for both our method and vanilla LoRA trained on the Aircraft, EuroSAT and Oxford Pets datasets in Fig. 9.

The results show that, compared to vanilla LoRA, our method tends to concentrate parameter updates on a more specific subset of transformer modules while reducing updates to pre-trained weights less relevant to the current data. This demonstrates that our method more effectively identifies critical

Table 9: Forgetting analysis. We report Backward Transfer (BWT) averaged across all X-TAIL tasks, where lower values indicate better retention.

Methods	ZSCL	MoE-Adapter	InfLoRA	LoRA ($r=4$)	LoRA ($r=8$)	LoRA ($r=16$)	CoDyRA
BWT (%) ↓	8.78	5.43	3.12	13.94	14.24	14.86	1.87

Table 10: Experimental results for integrating aggression-based adapters in the X-TAIL setting. Metrics for “Transfer”, “Average”, and “Last” are reported as averages across all datasets.

	Transfer	Average	Last
RAIL-Primal	62.4	70.7	79.1
CoDyRA + RAIL-Primal	63.1	74.1	83.4
RAIL-Dual	62.4	71.9	82.4
CoDyRA + RAIL-Dual	63.1	74.2	83.6

pre-trained weight matrices relevant to the current data and applies targeted dynamic parameter updates. Additionally, by reducing the strength of parameter updates for pre-trained weights less related to the current data, our method minimizes the impact on pre-trained knowledge and knowledge acquired from previous tasks compared to vanilla LoRA.

Note that this analysis differs from the visualizations of number of activated ranks in Fig. 5 and Fig. 6. The number of activated ranks reflects the quantity of significant ranks contributing to parameter updates for learning each task. In this analysis, the amplification factor directly measures the parameter change to each pre-trained weight matrix.

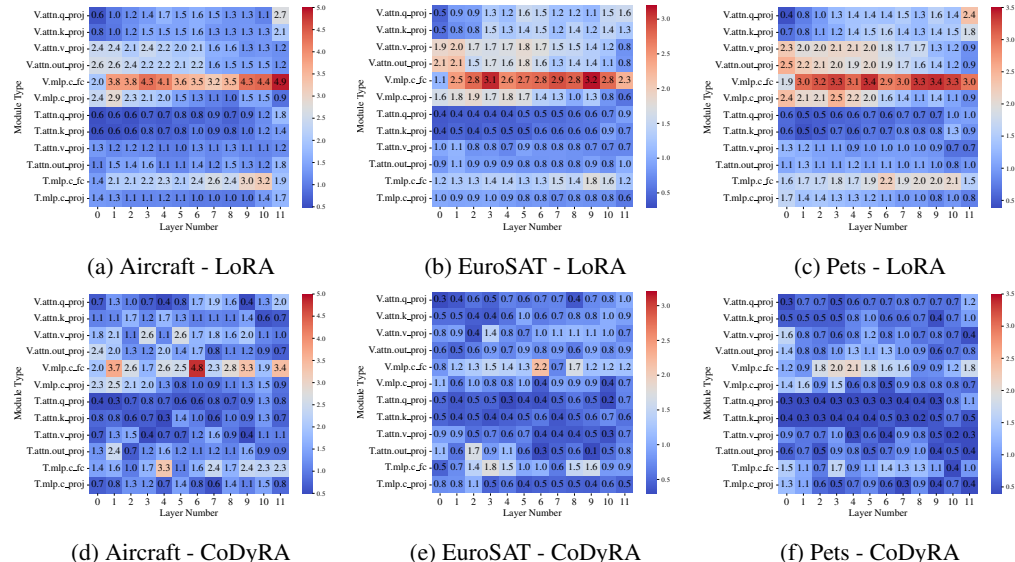


Figure 9: Visualization of amplification factors when trained on (a, d) Aircraft, (b, e) EuroSAT, and (c, f) Pets, comparing (d, e, f) our method of dynamic sparse rank selective LoRA and (a, b, c) vanilla LoRA. It shows that the proposed method with adaptive rank selection can achieve more focused/concentrated updating and less interference.

B.7 Parameter-space Directional Analysis

To further investigate how CoDyRA structures its parameter updates across sequential tasks, we conduct a parameter-space directional analysis following prior work on directional interference in LoRA-based continual learning. Specifically, we compute the cosine similarity between the LoRA A-matrix updates obtained after each task, comparing every task’s update direction against those from all other tasks. This metric captures the degree to which updates for different tasks align or interfere: higher similarity indicates that tasks induce overlapping update directions, while lower similarity reflects more orthogonal and thus less interfering modifications. As shown in Figure 10, CoDyRA consistently produces lower cross-task similarity than a baseline that trains a new LoRA adapter per task and merges them without additional constraints. Despite imposing no explicit orthogonality regularization, CoDyRA naturally encourages more decorrelated update directions, revealing an inherent structural property that helps mitigate destructive interference between tasks.

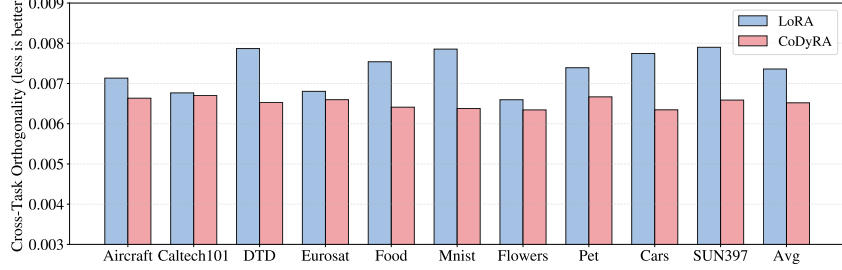


Figure 10: Parameter-space directional analysis of A-matrix updates. For each task, the column displays the average cosine similarity between the model’s LoRA updates after a specific task and the LoRA updates from models trained on all other tasks. This analysis quantifies directional interference among sequential updates. Lower cosine similarity reflects more orthogonal (less interfering) updates. CoDyRA produces lower similarity than the simple LoRA–merging baseline, demonstrating stronger implicit orthogonality of parameter updates even without explicit orthogonal regularization.

B.8 More Visualizations and Analyses on Rank allocation results of different datasets

In Sec. 4.2, Fig. 5 and Fig. 6, we visualize and analyze the dynamic ranks assigned to each module for the Aircraft and Oxford Pets datasets under the X-TAIL experimental settings. Here, we extend these visualizations and analyses to additional datasets, as shown from Fig. 11 to Fig. 18.

The visualizations, along with statistical analyses of transformer modules and layers, reveal distinct rank allocation patterns across datasets. These findings suggest that the rank of parameter updates needed for achieving a good downstream improvements and knowledge retention is distinct across each kind of data.

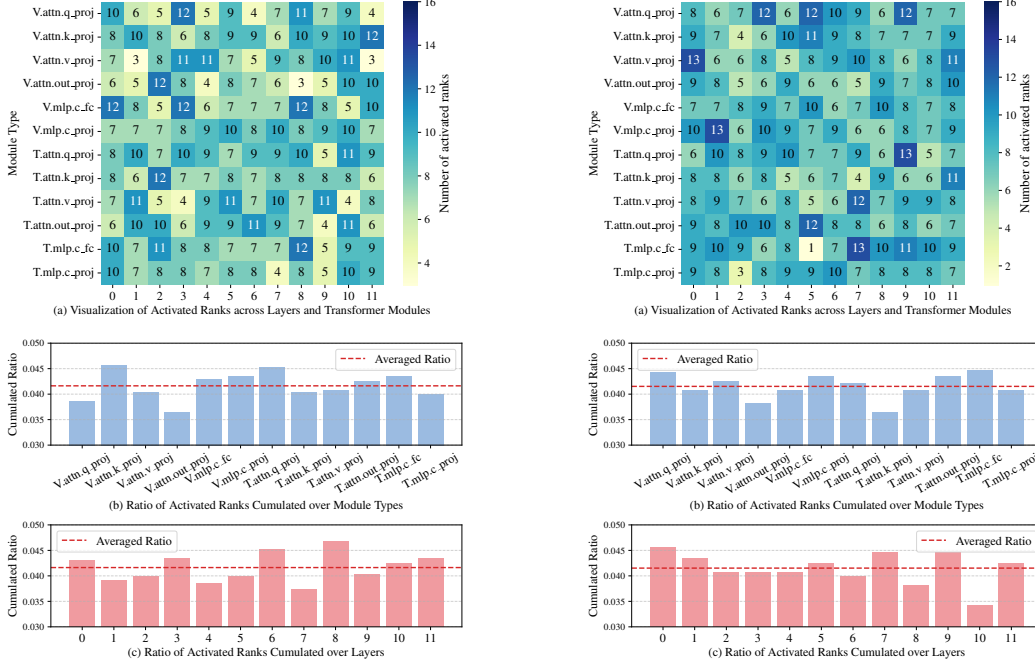
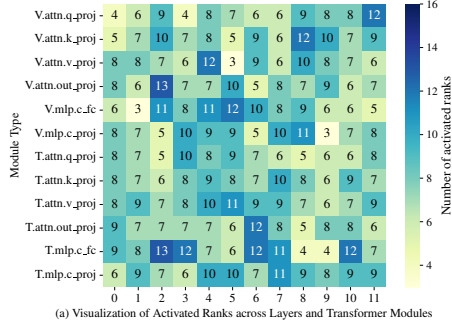


Figure 11: Visualization and statistical analysis of rank activation on the Caltech101 dataset using our proposed method.

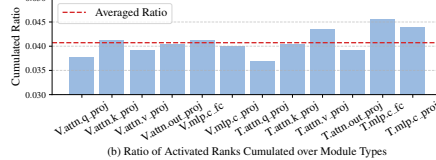
B.9 Evaluation with Other VLMs

To evaluate the broader applicability of our method, we conducted preliminary experiments with BLIP [37] on X-TAIL (Table 11). Our method consistently outperformed prior works and exceeded

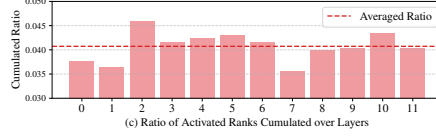
Figure 12: Visualization and statistical analysis of rank activation on the DTD dataset using our proposed method.



(a) Visualization of Activated Ranks across Layers and Transformer Modules

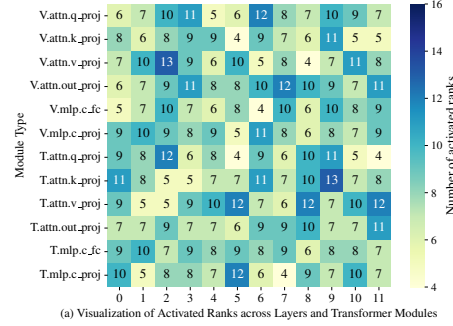


(b) Ratio of Activated Ranks Cumulated over Module Types

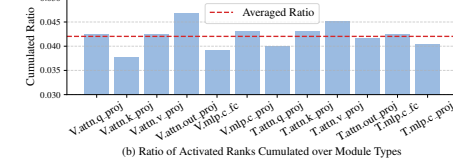


(c) Ratio of Activated Ranks Cumulated over Layers

Figure 13: Visualization and statistical analysis of rank activation on the EuroSAT dataset using our proposed method.



(a) Visualization of Activated Ranks across Layers and Transformer Modules



(b) Ratio of Activated Ranks Cumulated over Module Types

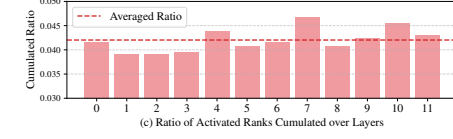


Figure 14: Visualization and statistical analysis of rank activation on the Flowers dataset using our proposed method.

Table 11: Averaged performance using BLIP.

	Transfer	Average	Last
Zero-shot	51.03	—	46.45
RAIL-Primal†	51.03	62.21	75.72
CoDyRA†	51.59	63.60	76.36

Table 12: Performance of 16-shot PEFT on downstream tasks.

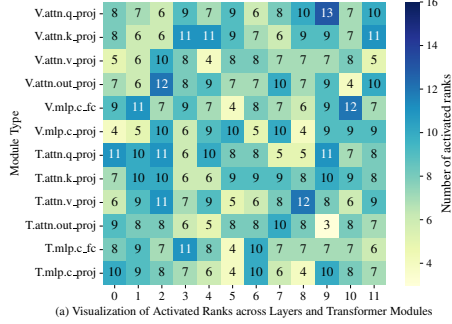
	Acc. ↑ / Final Used Params. ↓
	Caltech101 Cars OxfordPet
Zero-shot	88.40 64.70 89.00
LoRA ($r = 16$)	96.43 / 4.4M 80.66 / 4.4M 92.94 / 4.4M
CoDyRA ($r_{init} = 16$)	97.20 / 3.95M 81.61 / 3.75M 94.44 / 3.85M

the pre-trained model’s upper-bound performance, demonstrating its general effectiveness across different VLMs.

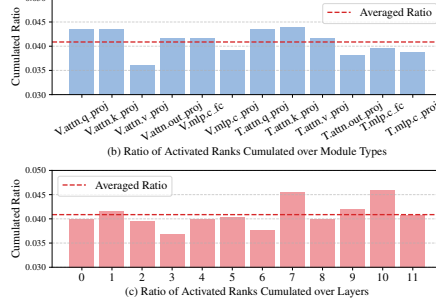
B.10 Evaluation on Standard Parameter-Efficient Fine-Tuning (PEFT) Task

Leveraging our dynamic rank-adaptive parameter updates, our method naturally extends to Parameter-Efficient Fine-Tuning (PEFT) tasks. Table 12 presents 16-shot PEFT results, using the same hyperparameters as the main paper, showing that CoDyRA outperforms vanilla LoRA while reducing final trainable parameters by pruning ranks with zero importance. Notably, across multiple downstream tasks (Caltech101, Cars, and OxfordPet), CoDyRA achieves higher accuracy while using fewer parameters compared to LoRA with a fixed rank of 16.

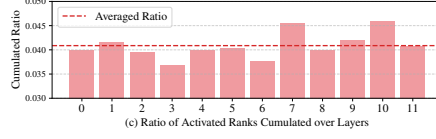
These results highlight a more adaptive and efficient alternative to conventional low-rank tuning by automatically selecting the most relevant ranks based on training data. Crucially, by amplifying



(a) Visualization of Activated Ranks across Layers and Transformer Modules



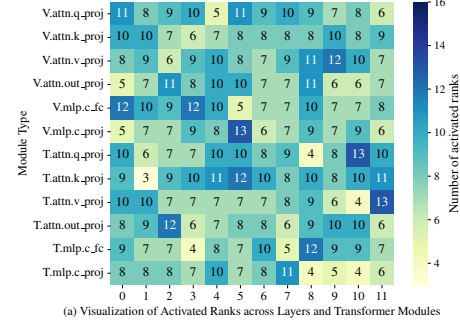
(b) Ratio of Activated Ranks Cumulated over Module Types



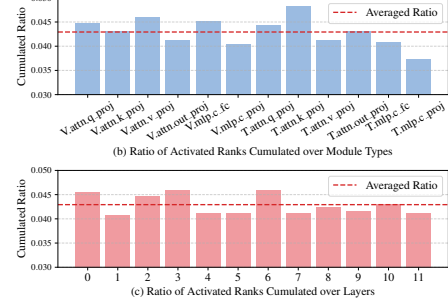
(c) Ratio of Activated Ranks Cumulated over Layers

Figure 15: Visualization and statistical analysis of rank activation on the Food101 dataset using our proposed method.

important ranks through learned higher importance weights, our approach significantly enhances downstream adaptation.



(a) Visualization of Activated Ranks across Layers and Transformer Modules



(b) Ratio of Activated Ranks Cumulated over Module Types

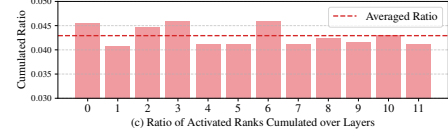
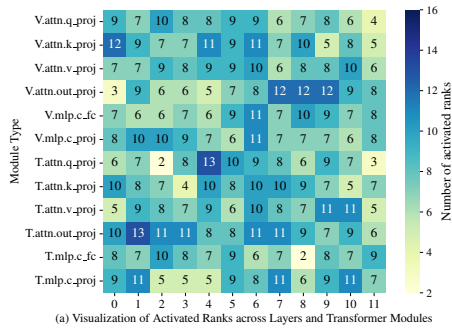
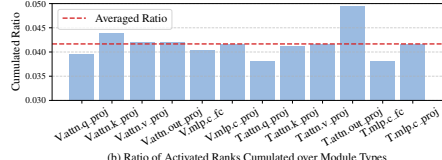


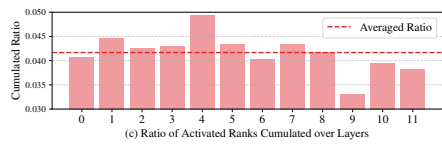
Figure 16: Visualization and statistical analysis of rank activation on the MNIST dataset using our proposed method.



(a) Visualization of Activated Ranks across Layers and Transformer Modules

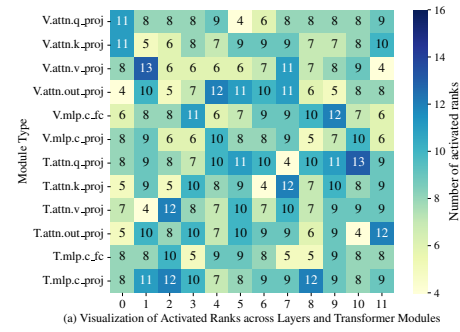


(b) Ratio of Activated Ranks Cumulated over Module Types

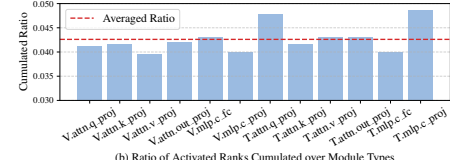


(c) Ratio of Activated Ranks Cumulated over Layers

Figure 17: Visualization and statistical analysis of rank activation on the Stanford Cars dataset using our proposed method.



(a) Visualization of Activated Ranks across Layers and Transformer Modules



(b) Ratio of Activated Ranks Cumulated over Module Types

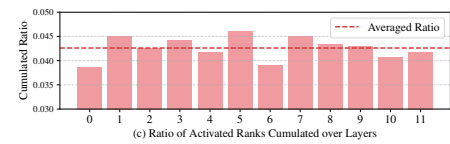


Figure 18: Visualization and statistical analysis of rank activation on the SUN397 dataset using our proposed method.